



Catchment characteristics control boreal mire nutrient regime and vegetation patterns over ~5000 years of landscape development

Betty Ehnvall ^{a,*}, Anneli M. Ågren ^a, Mats B. Nilsson ^a, Joshua L. Ratcliffe ^b, Koffi Dodji Noumonvi ^a, Matthias Peichl ^a, William Lidberg ^a, Reiner Giesler ^c, Carl-Magnus Mörth ^d, Mats G. Öquist ^a

^a Department of Forest Ecology and Management, Swedish University of Agricultural Sciences, Skogsmarksgränd 17, 90183 Umeå, Sweden

^b Unit for Field-Based Forest Research, Swedish University of Agricultural Sciences, 922 91 Vindeln, Sweden

^c Climate Impacts Research Centre Umeå, Sweden, Department of Ecology and Environmental Sciences, Umeå University, 90736 Umeå, Sweden

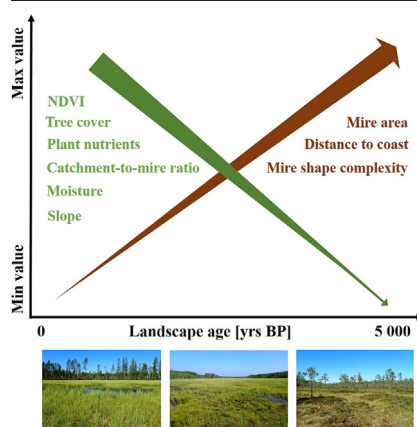
^d Department of Geological Sciences, Stockholm University, Svante Arrheniusväg 8, 10691 Stockholm, Sweden



HIGHLIGHTS

- Quantitative description of landscape controls on mire vegetation patterns.
- Satellite based NDVI used to describe vegetation in open and tree-covered mires
- Long-term mire development assessed by applying a mire chronosequence approach
- Catchment controls peat nutrient concentrations, and further, vegetation patterns.
- Lower mire NDVI in older parts of the landscape

GRAPHICAL ABSTRACT



ARTICLE INFO

Editor: Jan Vymazal

Keywords:

Catchment support
Chronosequence
NDVI
Landscape ecology
Holocene

ABSTRACT

Vegetation holds the key to many properties that make natural mires unique, such as surface microtopography, high biodiversity values, effective carbon sequestration and regulation of water and nutrient fluxes across the landscape. Despite this, landscape controls behind mire vegetation patterns have previously been poorly described at large spatial scales, which limits the understanding of basic drivers underpinning mire ecosystem services. We studied catchment controls on mire nutrient regimes and vegetation patterns using a geographically constrained natural mire chronosequence along the isostatically rising coastline in Northern Sweden. By comparing mires of different ages, we can partition vegetation patterns caused by long-term mire succession (<5000 years) and present-day vegetation responses to catchment eco-hydrological settings. We used the remote sensing based normalized difference vegetation index (NDVI) to describe mire vegetation and combined peat physicochemical measures with catchment properties to identify the most important factors that determine mire NDVI. We found strong evidence that mire NDVI depends on nutrient inputs from the catchment area or underlying mineral soil, especially concerning phosphorus and potassium concentrations. Steep mire and catchment slopes, dry conditions and large catchment areas relative to mire areas were associated with higher NDVI. We also found long-term successional patterns, with lower NDVI in older mires. Importantly, the NDVI should be used to describe mire vegetation patterns in open mires if the focus is on surface vegetation, since the canopy cover in tree-covered mires completely dominated the NDVI signal. With our study approach, we can

* Corresponding author.

E-mail address: betty.ehnvall@slu.se (B. Ehnvall).

<http://dx.doi.org/10.1016/j.scitotenv.2023.165132>

Received 18 April 2023; Received in revised form 21 June 2023; Accepted 23 June 2023

Available online 26 June 2023

0048-9697/© 2023 The Authors. Published by Elsevier B.V. This is an open access article under the CC BY license (<http://creativecommons.org/licenses/by/4.0/>).

quantitatively describe the connection between landscape properties and mire nutrient regime. Our results confirm that mire vegetation responds to the upslope catchment area, but importantly, also suggest that mire and catchment aging can override the role of catchment influence. This effect was clear across mires of all ages, but was strongest in younger mires.

1. Introduction

High-latitude mires comprise one of the most important carbon stores globally, holding ~80 % of the global peatland carbon stock (Hugelius et al., 2020; Loisel et al., 2014). These ecosystems are also crucial for local biodiversity (Joosten and Clarke, 2002) and downstream water quality through the regulation of water and nutrient exports (Fergus et al., 2017; Helbig et al., 2020a, 2020b; Lane et al., 2018; Sponseller et al., 2018). Many of the services provided by mires depend on local mire vegetation patterns which are in turn related to species composition and plant productivity. Thus, identifying the drivers behind mire vegetation patterns is necessary to understand how mire processes and functions are regulated by the surrounding landscape.

General vegetation patterns at the landscape, as well as more local scales, can be monitored using remote sensing-based vegetation indices. A commonly applied index is the normalized difference vegetation index (NDVI; Pettorelli, 2013), which is based on the spectral ratio between the visible red (Red; central wavelength 665 nm) and near-infrared (NIR; central wavelength 842 nm) wavelengths (Rouse et al., 1973). The NDVI can be calculated from any multispectral image containing these bands, such as aerial photographs or satellite images (Räsänen et al., 2020). The NDVI has been suggested as a powerful proxy for the net primary productivity (NPP) in various biotopes, including mires (Boelman et al., 2003; McPartland et al., 2019), and has been confirmed by field validation and laboratory experiments (Lees et al., 2020). Under certain conditions, however, the use of NDVI as a proxy for mire productivity is less appropriate. For example, during drought *Sphagnum* mosses have a higher NIR reflectance, leading to higher NDVI (Lees et al., 2019), without concomitant response in photosynthetic rate and primary productivity. Moreover, estimates of mire productivity based on NDVI in *Sphagnum* dominated mires can be overestimated because of the lower contemporary photosynthetic capacity in these mosses compared to vascular plants (Yuan et al., 2014). While the NDVI has been repeatedly used to describe mire vegetation patterns (e.g. Anderson et al., 2021; Järveoja et al., 2018; Mzobe et al., 2018), catchment scale drivers behind the vegetation patterns, as reflected in the NDVI, have been poorly described in the scientific literature.

Mire vegetation ranges from purely aquatic species, through semi-aquatic plants such as *Sphagnum* mosses that can be seasonally inundated, depending on the species (Granath et al., 2010; Gunnarsson, 2005; Laine et al., 2011), to purely terrestrial plants such as ericaceous dwarf shrubs and trees, typically *Betula* sp. and *Pinus sylvestris* (Moor et al., 2017; Rydin et al., 2013). If micro-topographic gradients have developed within a mire (Eppinga et al., 2010; Glaser et al., 1990), aquatic species may be found in mire pools, semi-aquatic species in hollows and lawns, and terrestrial species on hummocks (Moor et al., 2017; Rydin et al., 1999). Examples of such structured ecosystems are mire complexes, or aapa mires, which may comprise large areas of distinct vegetation types. If mires, on the other hand, represent diverse hydrologic and/or nutrient regimes, different plant functional types will be found at different mires (Diamond et al., 2021; Gunnarsson et al., 2014). Nutrient regime we here define as an ecological indicator of plant available nutrients, which are defined by the inflow, accumulation and transformation of nutrients in the mire (Zhao et al., 2013).

The mires nutrient regimes determine vegetation patterns at the local scale, including both the mire plant community composition and productivity (Økland et al., 2001; Peichl et al., 2018). The link between nutrient regime and mire vegetation patterns is reflected in mire NDVI, as local studies have shown (Loiko et al., 2020), but this has not been confirmed at large

spatial scales. Based on the hydrological connection to supporting upland areas, mires have long been categorized as minerogenic (fens) or ombrogenic (bogs; Sjörs and Gunnarsson, 2002). Strictly, ombrogenic mires receive water from precipitation, with dissolved or particulate nutrients therein, while nutrient regimes in minerogenic mires in addition are influenced directly from the underlying mineral soil or from dissolved nutrients from the upland supporting catchment area (Ivanov, 1981; Romanov, 1968). Because of these additional external nutrient sources, minerogenic mires can be more nutrient rich compared to ombrogenic mires, although the nutrient spectra of minerogenic mires ranges from poor (oligotrophic) to rich (eutrophic), depending on the nutrient content on the groundwater feeding into the mire (Avetov et al., 2021). In this study, we focus on minerogenic mires since these represent the majority of mire areas in Scandinavia and at high latitudes generally.

The variation in nutrient conditions in minerogenic mires is reflected in a large variation in plant community composition, spanning from species adapted to nutrient poor conditions (e.g. nutrient conservative *Sphagnum* mosses) to species adapted to rich conditions (e.g. nutrient acquisitive vascular plant species; Laine et al., 2021). An important process that could potentially shift mires from eutrophic to oligotrophic is changed nutrient transfer rates from the upslope catchment area. This may result in successional differences in mire vegetation over time (Martini and Glooschenko, 1985). It is worthwhile noting, though, that the regolith thickness can be more important than weathering rate for nutrient export and thus plant nutrient availability (Maher and von Blanckenburg, 2023). Differences in the catchment supply of nutrients to mire vegetation is also strongly influenced by the catchment eco-hydrological settings (Mäkilä et al., 2015) and this is likely also important for the vertical and horizontal distribution of elements across any mire-rich landscape, although this needs confirmation.

To address the presented knowledge gaps, we use NDVI to describe responses in mire vegetation patterns to the biogeochemical catchment support over the late Holocene. While NDVI is a common proxy for vegetation patterns, it is important to use ground measurements and other remotely sensed indices to validate results obtained from NDVI. In our case, we are specifically interested in how mire NDVI relate to macro and micronutrients concentrations in the surface peat. Moreover, we present an approach to scale-up NDVI responses to the catchment support from the individual sampling point level to the landscape level using remote sensing data. The concomitant effect of landscape aging, including slower weathering rates of mineral soil in older landscapes (Starr and Lindroos, 2006), is impossible to study in many parts of the world. The area we used to address these research questions is a natural post-glacial isostatic rebound mire chronosequence in northern Sweden. Here, new land has been exposed from the sea since the retreat of the Scandinavian Ice Sheet from the area ~10,000 cal. years BP (Stroeven et al., 2016), today at a rate of ~9 mm yr⁻¹ (Nordman et al., 2020). Moving from the present coastline, along the mire chronosequence, to the inland (15 km from the coastline) provides a unique opportunity to explore the temporal variability in catchment controls on mire NDVI and mire succession over the Holocene time-scale (Svensson and Jøglum, 2001; Tuittila et al., 2013; Walker et al., 2010). Ehnvall et al. (2023) provide a more detailed description of the chronosequence approach in the Bothnian Bay area. We use the following research questions to address the identified knowledge gaps:

- Q1. Does NDVI reflect the variation in surface peat nutrient concentrations in boreal mires?
- Q2. Can we describe variation in mire NDVI based on ecohydrological catchment characteristics?
- Q3. How is mire NDVI controlled by Holocene landscape age?

2. Materials and methods

We applied three different spatial scales to address the research questions: 1) mire sampling point level, 2) whole-mire level based on the sampled mires, and finally, 3) the extended mire population at the landscape level (Fig. 1). From now on, we refer to the three levels as “point”, “mire” and “landscape”. At point level, we studied within-mire responses of NDVI to the catchment support by combining NDVI with measured peat physico-chemical and topographic properties ($n = 135$). From there, we scaled up to the mire level based on the sampled mires ($n = 47$), and described among-mire NDVI response to catchment eco-hydrological settings using various remote sensing based terrain attributes and attributes describing mire geometry and age. Finally, at the landscape level, we applied the same terrain attributes as for the mire level, but scaled up to mires interlaying, and including, the sampled mires in the chronosequence area ($n = 1576$).

2.1. Chronosequence settings

Our $\sim 550 \text{ km}^2$ study area ($63^\circ 40' - 64^\circ 10' \text{ N}$, $20^\circ 20' - 20^\circ 50' \text{ E}$) is part of the Sävar Rising Coastline Mire Chronosequence (SMC) in the Swedish province of Västerbotten in the Bothnian Bay Lowlands (BBL; Fig. 1). The studied mires were distributed along an age gradient from the present coastline to $\sim 60 \text{ m}$ above sea level (m.a.s.l.), corresponding to a land surface age range of $\sim 0 - 5000$ years BP (Renberg and Segerström, 1981). The maximum distance inland among the studied mires is $\sim 15 \text{ km}$.

The direction of the ice retreat has formed elongated landscape features consisting of wave-exposed and till covered ridges interlaid by valleys covered by finer minerogenic deposits, mainly of postglacial silt, clay and sand (Lindén et al., 2006). Lacustrine and glacio-lacustrine sediments are found along river Sävar. The bedrock is dominated by paragneiss (predominately made up of quartz, feldspar and mica), but felsic (granodiorite, granite) and

mafic rock intrusions (basaltic andesite, gabbrodiorite) are also found, according to bedrock maps (1: 50,000) by the Geological Survey of Sweden. The gently undulating landscape settings are suitable for mire initiation, expansion and succession (Ecke and Rydin, 2000; Ehnvall et al., 2023). Today, around 25 % of the land area in the region is covered by mires, with higher mire cover in the more inland, older, parts of the study area (Ehnvall et al., 2023). The mire population is completely dominated by minerogenic fens (Gunnarsson et al., 2014).

The present annual averages for temperature and precipitation over the current 30-year reference period (1991–2020) are 3.5° C (July 15.7° C , January -6.8° C) and 654 mm (July 79 mm and January 48 mm ; The Swedish Meteorological and Hydrological Institute, 2022). Temperatures and precipitations are based on mean values from the meteorological stations closest to the study area (Umeå airport and Vindeln-Sunnansjönäs).

We defined mire areas in the chronosequence based on a mire layer in the Swedish Property Map (1: 10,000, Swedish Mapping, Cadastral and Land Registration Authority, Lantmäteriet), since this is the currently most detailed mire map in Sweden. Mire segments that were split by roads were merged and ponds with open water included in the mire objects before we performed any further analyses. Mires on floodplains along the river Sävar were also identified and excluded, as these might represent mires with different genesis and hydrology (Lane et al., 2018).

2.2. Peat properties

2.2.1. Sampling

We sampled 47 mires along two chronosequence trajectories separated by the Sävar river (Fig. 1). No ditches were crossing the mire surface within $\sim < 50 \text{ m}$ from the sampling point, and hence, effects on possible mire ditches on the surface peat properties are practically negligible (Bring et al., 2022). The mires were distributed evenly across the age gradient

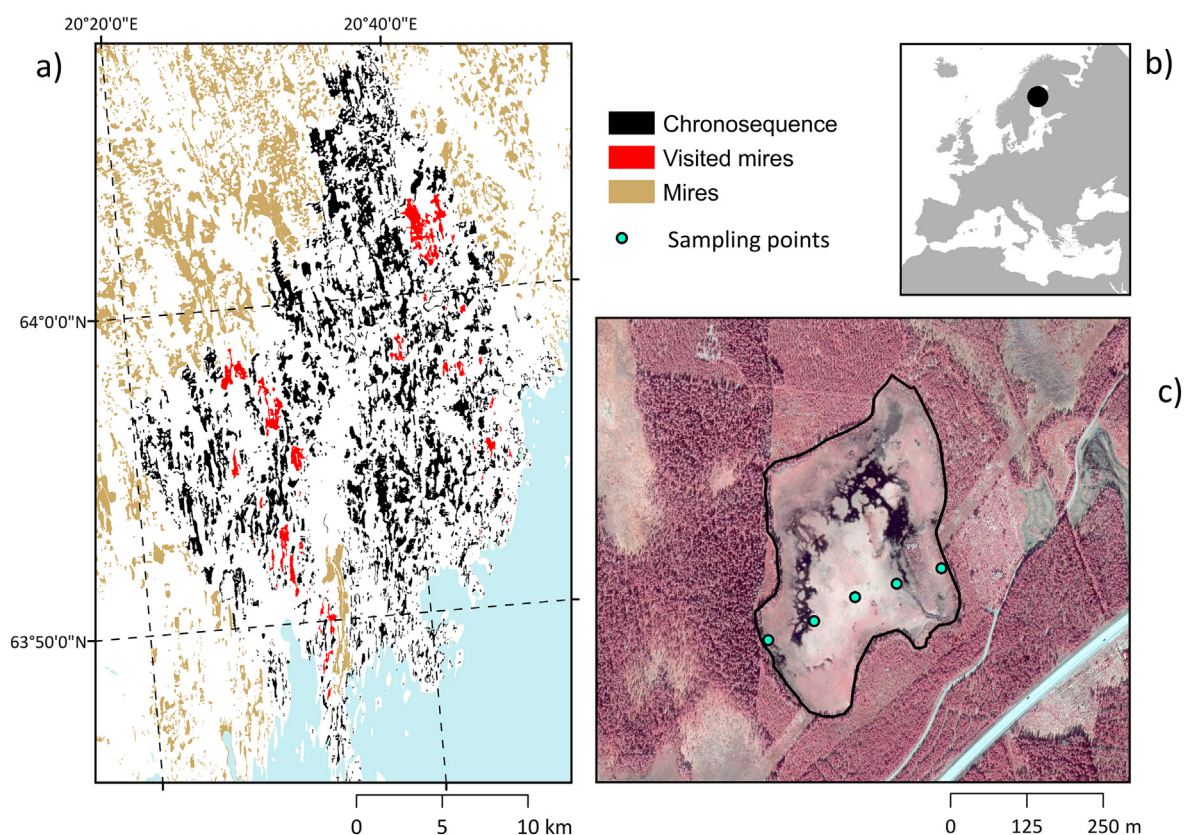


Fig. 1. (a) The studied mires are found in the 0–60 m.a.s.l. range in a coastal area of Northern Sweden (b), with the closest distance from any point on the mire surface to the present coastline of maximum 15 km. Mires used for analyses at the landscape level, using only GIS data, are marked in black (a), while mires that were sampled in the field are marked in red (a). At the point level, we applied sampling transects with five edge-to-edge points (c). In c) a high-resolution infra-red aerial photograph is used to depict the mire, although importantly, in the NDVI extraction, we used $10 \times 10 \text{ m}$ resolution Sentinel-2A satellite images.



Fig. 2. Example photos from six mires (IDs provided in the lower right corner) sorted according to mire elevation from the lowest (ID 1156 at ~2 m.a.s.l.) in the upper left corner to highest (ID 2346 at ~53 m.a.s.l.). All mires can be visited in the interactive mire chronosequence map <https://slughg.github.io/MiresChrono>.

and represent mires of different sizes (Fig. 1). The same 47 mires were also included in the mire level analyses based on remotely sensed GIS data.

We used edge-to-edge sampling transects, comprising five sampling points each. Edge points were located 10 m from the mire edges, center point in the middle of the transects and intermediate points between the center point and the edge points (Fig. 1c). We defined the mire edge in the field based on vegetation and peat depth (> 30 cm peat), and located the sampling point further out in the mire expanse based on the position of the edge points. At small mires, the edge points were placed 5 m from the mire edge due to

short distance across the mire. With two fixed edge points and three mire distance dependent points, the sampling strategy is semi-fixed and proportional to the distance across the mire area. To minimize slope effects, as well as possible age gradients in large mire complexes, all transects were located perpendicular to the direction of the isostatic rebound. We provide photos (Fig. 2) from all mires and sampling points in our interactive mire chronosequence map (<https://slughg.github.io/MiresChrono>).

We collected peat samples from the mires between 2 July and 30 August 2018, and visited the mires in random order to avoid temporal bias

Table 1

Summary of point level data. The spatial resolution is provided when relevant.

Index	Description	Spatial resolution	Source
Peat physical properties			
BD [g cm^{-3}]	Dry bulk density	2–5 sampling points per mire transect	Peat sample
Cond. [μScm^{-1}]	Electrical conductivity	--:--	Peat sample
Depth [cm]	Peat depth	--:--	Field measurement
DM [%]	Dry matter content	--:--	Peat sample
LOI [%]	Loss on ignition	--:--	Peat sample
pH	pH	--:--	Peat sample
Peat chemical composition			
Al, C, Ca, Cr, Cu, Fe, K, Mg, Mn, Mo, N, Na, Ni, P, S, Se, Si, Zn [mg g^{-1}]	Elemental concentration in 10 cm surface peat. For the statistical analyses, z-scores are used.	14 full transects (70 samples), 33 mid-edge pairs (66 samples)	ICP-OES ^a , ICP-SFMS ^b and Elemental analyzer (Flash EA 2000)
GIS data			
Coast_dist [m]	Distance from the sampling point to any point along the present coastline.		Swedish Mapping, Cadastral and Land Registration Authority
Edge_dist [m]	Distance from the sampling point to any point along the mire polygon margin.	1:10000	Swedish Mapping, Cadastral and Land Registration Authority
Elevation [m.a.s.l.]	Sampling point elevation above sea level.	2×2 m	DEM ^c , Swedish Mapping, Cadastral and Land Registration Authority
NDVI	Sampling point normalized difference vegetation index	10×10 m	Calculated from Sentinel-2 Level 2A, European Space Agency
Pos()	Position along the sampling transect: edge, intermediate or center		
TWI	Sampling point topographic wetness index	24×24 m	Calculated from DEM ^c , Swedish Mapping, Cadastral and Land Registration Authority
Vol. [$\text{m}^3 \text{ha}^{-1}$]	Sampling point tree standing volume	12.5×12.5 m	SLU Forest Map, Dept. of Forest Resource Management, Swedish University of Agricultural Sciences

^a Inductively Coupled Plasma Optical Emission Spectrometry.

^b Inductively Coupled Plasma Mass Spectrometry.

^c Digital Elevation Model.

associated with the geographical position of a mire. All sampling points were mapped using a Trimble GeoExplorer 6000 GPS with a vertical and horizontal precision of 0.02 m.

2.2.2. Peat physical properties

We measured peat depth manually at each transect point by pushing a metal rod into the peat until it reached a non-penetrating surface. We extracted 10 cm deep surface peat cores, with a surface area of 6×6 cm, for analyzing dry bulk density (BD), dry matter content (DM; 105 °C for 24 h), loss on ignition (LOI; 550 °C for 6 h) and chemical composition (see below). We identified the interphase between the living vegetation and peat surface in the field based on the vegetation structure, and removed the living part. In addition, we collected a separate peat sample for pH (Greisinger GMH5530) and conductivity (INESA DDS-307) measurements from the same peat depth. The peat samples were kept in plastic bags and stored in a freezer (−19 °C) within 8 h after extraction. We provide detailed information about the peat physical measurements in the Supporting Information (A).

2.2.3. Peat chemical composition

To reflect mire nutrient regimes across the mires, we analyzed dried peat samples for total elemental concentrations of aluminum (Al), carbon (C), calcium (Ca), chromium (Cr), copper (Cu), iron (Fe), potassium (K), magnesium (Mg), manganese (Mn), molybdenum (Mo), nitrogen (N), sodium (Na), nickel (Ni), phosphorus (P), sulfur (S), selenium (Se), silicon (Si) and zinc (Zn; Table 1).

The peat samples were oven dried (60 °C for three days) and larger roots (diameter > 1 mm) were removed before we ground the samples (1–3 min, depending on the substratum, with rotating speed of 25,000 rpm,) using an IKA mill (20000005401), with disposable tubes (20000005402). We analyzed the elemental compositions of peat from a subset of the transect samples ($n = 136$). Mass fractions of total carbon and nitrogen were analyzed using Elemental analyzer (Flash EA 2000, Thermo Fisher Scientific). For the other elements, we used two different labs, digestions methods and analytical instruments. For 14 of the mires peat samples from full transects, in total 70 samples, were measured using Inductively Coupled Plasma Optical Emission Spectrometry (ICP-OES), while from 33 mires pairs of mid and edge samples, in total 66 samples, were analyzed using Inductively Coupled Plasma Sector Field Mass Spectrometry (ICP-SFMS). Details about the peat extraction techniques are provided in the Supporting information (A).

Of the samples measured using ICP-OES, 14 samples were replicated with ICP-SFMS, to validate comparison of the two measurement techniques. For samples analyzed with both ICP-OES and ICP-MS, we used the results from ICP-OES in the later modelling. Overall, most elements in the comparison agreed well between the two methods ($R^2 = 0.91$ – 0.99 for Al, Fe, Ca, Mg, P, S), while the remaining were somewhat weaker related (Cu $R^2 = 0.88$; K, $R^2 = 0.82$; Na $R^2 = 0.75$; Zn $R^2 = 0.64$ and Si $R^2 = 0.56$). The slope was on average 0.7 (Si not included). Silica was threefold higher when determined by ICP-OES compared to ICP-SFMS. Due to the offset between the two datasets, we calculated z-scores (Eq. (1)) based on the mean (μ) and standard deviations (σ) of the population of each of the elements before pooling the datasets based on the two approaches, before proceeding with statistical analysis. One sampling point had more than one order of magnitude higher concentrations for several of the elements of interest. The outlier was excluded from the dataset before z-scores were calculated.

$$z = \frac{x - \mu}{\sigma} \quad (1)$$

2.3. Mire vegetation

2.3.1. Tree standing volume

We used the tree standing volume (Vol., [$\text{m}^3 \text{ha}^{-1}$]) to separate open sampling points from tree covered sampling points (point level analyses), as well as open mires from tree-covered mires (mire and landscape level analyses). The tree standing volume was based on a national forest map from 2015 (SLU Forest Map. Dept. of Forest Resource Management, Swedish University of Agricultural Sciences), with a raster resolution of 12.5×12.5 m. At the

point level, we separated open and tree-covered points based on the pixel overlying the sampling points. At the mire and landscape levels, we classified mires with a median standing volume of $0 \text{ m}^3 \text{ha}^{-1}$ as open mires, while all other mires were classified as tree-covered (Table E.1).

2.3.2. Excluding heavily drained mires from the landscape level mire population

Based on a national ditch map, we defined the level of mire drainage in all mires included in the study (landscape level). The applied ditch map was created using deep learning (Lidberg et al., 2023) and classified each 1×1 m cell across the landscape into a ditch or non-ditch (Laudon et al., 2022). We calculated the total number of stream pixels (both natural streams and ditch cells) and normalized it to the mire area. We excluded heavily drained mires with >0.02 ditch pixels per square meter, corresponding to $>2\%$ of the 1×1 m pixels across the mire area, as human impact would risk considerable impacts on the mire vegetation at these sites. After removing heavily drained mires (1246 mires), the mire population at the landscape level comprised 1576 mire objects that were either undrained (0 ditch pixels per square meter) or moderately drained, with <0.02 ditch pixels per square meter (Fig. 1, Table E.1).

2.3.3. NDVI calculation

In Google Earth Engine (Gorelick et al., 2017), we extracted monthly NDVI data at point, mire and landscape levels. Inter-annual variation in weather conditions and groundwater levels could result in different catchment responses on NDVI during different vegetation periods if, for example, the timing of mire green-up (Antala et al., 2022) or peak season (Crichton et al., 2022) diverges or if mire plants were affected by summer drought (Rinne et al., 2020). We reduced possible impacts of inter-annual, phenological variability in NDVI by using the most recent available NDVI extraction procedures available in Google Earth Engine, and further, by averaging NDVI over six vegetation periods (April – November 2017–2022), using harmonized atmospherically corrected satellite images from the European Space Agency's Sentinel 2-mission (Level 2A). Details about the NDVI extraction, along with a link to the scripts on GitHub, are provided in the Supporting Information (B).

Across the chronosequence, we found a progression in mire NDVI over the vegetation period, typical of northern peatlands, with low NDVIs during the spring green-up phase, progressively higher NDVIs during the peak growth and decreasing NDVIs as the vegetation approach senescence (Fig. 3;

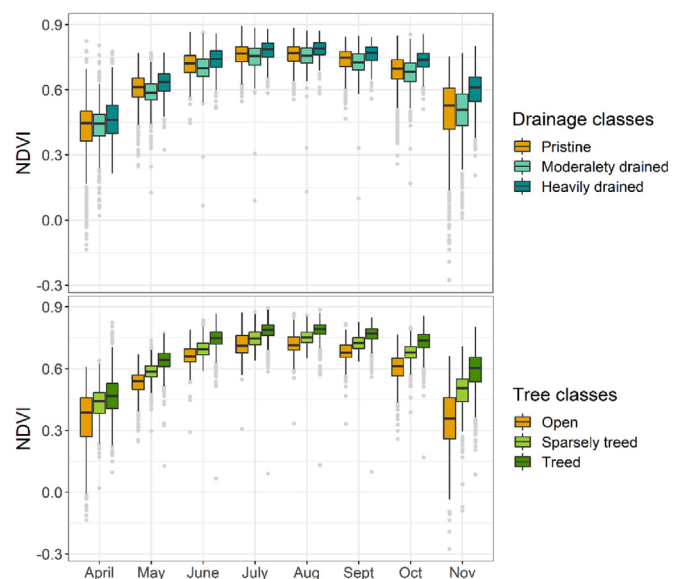


Fig. 3. Temporal variability in the normalized difference vegetation index (NDVI) for all mires in the chronosequence area. Each point represents the mean mire NDVI for the different months (April–November). Pristine mires comprise no ditch cells, moderately drained mires <0.02 ditch pixels per square meter and heavily drained mires >0.02 . Open mires have a median stand volume of 0, sparsely tree-covered mires $<50 \text{ m}^3 \text{ha}^{-1}$ and tree-covered mires $>50 \text{ m}^3 \text{ha}^{-1}$.

Eklundh et al., 2011; McPartland et al., 2019). For the further analyses we focus on May–September, which reflects the three phases of the vegetation period (green-up = May–June, peak growth = July–August and senescence = September).

2.4. Mire catchments

2.4.1. Catchment delineation

We defined the catchment as upslope areas that are hydrologically connected to the mire through flow paths and, further, separated the total catchment from the unique catchment. The total catchment (TC) represents all upslope areas, while the unique catchment (UC) represents upslope areas that the mire does not share with any upslope mires. We focus primarily on the unique catchment, since upslope mires can immobilize weathering products, thus, making the mires retention hotspots (Cohen et al., 2016). From now on, the unique catchment is referred to as “the catchment” if nothing else is stated.

We delineated total and unique catchments for the mires (mire and landscape level) using the open-source GIS system Whitebox Geospatial Analysis Tools. We used a national 2×2 m digital elevation model (DEM) based on LiDAR scanning with 0.5–1 points per square meter and a vertical resolution of 0.3 m and horizontal resolution of 0.1 m (The Swedish Mapping, Cadastral and Land Registration Authority). We provide details about the catchment delineation, along with a link to the script on GitHub, in the Supporting Information (C).

2.4.2. Catchment age

To describe succession within the chronosequence, we calculated land surface age (T_{age}) from the 2×2 m DEM (z) and a local shore displacement curve based on six varved lake sediments in the 29–177 m.a.s.l. elevation range (Eq. (2); Renberg and Segerström, 1981). Varved lake sediments allow for both identifying the transition from marine to lacustrine sediments and also to date this transition.

$$T_{age} = -0.287z^2 + 99.967z \quad (2)$$

From the obtained age distributions, we extracted mean ages of all unique catchments (mire and landscape level). The age corresponds to the time the catchment area has been uplifted from the sea and, hence, exposed to weathering. Mire initiation can lag land availability depending on the mire initiation type (primary mire formation, terrestrialization or paludification; Ruppel et al., 2013) and dispersal of plant species (Tiselius et al., 2019). Because of this, we use elevation and the shortest distance from the sampling points (point level) or any point in the mire polygon (mire and landscape levels) to the present shoreline, instead of land surface age, to indicate the position of the points and mires in the chronosequence.

2.4.3. Mire and catchment geometry

We describe the mires and their catchments using various morphological and hydrological terrain attributes (mire and landscape level; Table 2). First, we extracted areas of the mires and their total and unique catchments using SAGA v. 7.9.0 (Conrad et al., 2015), and calculated the areal ratios between the mire and the unique catchment (UC-to-mire; Eq. (3)), as well as the ratio between the unique and the total catchment (UC-to-TC; Eq. (4)). UC-to-mire reflects the hydrological catchment support, where a higher ratio implies that a mire unit area is potentially supported by a larger catchment unit area relative to a lower ratio. The UC-to-TC, on the other hand, can be interpreted as the biogeochemical catchment support, where a lower ratio reflects upslope located mires that may act as biogeochemical sinks to downslope located mire.

$$UC - to - mire = \frac{Catchment\ area}{Mire\ area} \quad (3)$$

$$UC - to - TC = \frac{Unique\ catchment\ area}{Total\ catchment\ area} \quad (4)$$

Further, we describe mire geometry using the shape index, which illustrates the complexity of the mire's two-dimensional shape (Eq. (5); Forman and Gordon, 1986). In the shape index calculation, the perimeter of the mire (P) is compared with the perimeter of a circle with equal area (A). A circular mire, with a shape index of 1, has the largest interior area compared to its perimeter. The more a mire shape deviated from a circle, the more the shape index deviates from 1. In addition to describing the complexity of the two-dimensional mire shape, we also get an estimate of possible fragmentation and edge effects on the mire plant communities using the shape index (Soomers et al., 2013).

$$Shape\ index = \frac{P}{2 * \sqrt{(A * \pi)}} \quad (5)$$

2.4.4. Mire and catchment hydrology

We describe local topographic and hydrologic conditions using the mean mire (Mire slope) and catchment (UC slope) slopes. Slope (%) was calculated from the $2 \text{ m} \times 2 \text{ m}$ DEM according to Zevenbergen and Thorne (1987) in SAGA GIS v. 7.9.0. High values represent steep slopes.

To describe moisture conditions in the upslope catchment areas, we used a recently developed national soil moisture index (Ågren et al., 2021). The soil moisture index is based on a machine-learning algorithm, with input data such as terrain attributes at different scales, for example the topographic wetness index (TWI; Beven and Kirkby, 1979) and depth-to-water (Murphy et al., 2011), soil properties (e.g. soil depth and Quaternary deposit type), as well as runoff indicators (Ågren et al., 2021). The algorithm was trained and validated on moisture data from c. 20,000 soil plots distributed across Sweden. The index represents the likelihood that a pixel in the 2×2 m mapped landscape is wet (0 = dry, 100 = wet). We expect moister catchments to comprise peat soils (Ågren et al., 2022), while drier catchments may comprise upland soils with shallow humus layers.

Since the soil moisture index was primarily developed to describe moisture in forested areas, and since mire areas are included as input data in the algorithm, we did not use the soil moisture index to describe mire moisture. Instead, mire moisture was described using the topographic wetness index (TWI; Table 1; Beven and Kirkby, 1979). TWI describes the propensity of each cell to be saturated to the soil surface, and is calculated based on the slope ($\tan b$), representing drainage conditions at the site, and the contributing area (a):

$$TWI = \ln \frac{a}{\tan b}$$

We expect mires with high TWI scores to be wet due to large contributing areas and gentle slopes, while sites with low TWI values are expected to be better drained and, consequently, drier. TWI performs better when calculated on a coarser resolution (Larson et al., 2022) and was calculated on a 24×24 m resolution. More details about the TWI calculation is provide in the Supporting Information (D).

2.4.5. Catchment geology and land use

We used maps from the Geological Survey of Sweden to calculate percentages of different bedrock classes (felsic, felsic-intermediate, intermediate, mafic) and Quaternary deposits (till, coarse, sand, clay-silt) within the catchments. From the Swedish Property map (1: 10,000, Swedish Mapping, Cadastral and Land Registration Authority, Lantmäteriet), percentages of land cover and land use classes were extracted. Within the catchments, arable land, coniferous forest, deciduous forest and open areas were present. Open areas include areas with a vegetation height below 1.5 m such as abandoned agricultural lands, low-productive grazing areas, heaths and meadows and bedrock outcrops.

2.5. Statistical analyses

The aim of this study was to identify mire NDVI responses to catchment characteristics and landscape aging. Therefore, we chose the OPLS (orthogonal projections to latent structures; Eriksson et al., 2006) method,

Table 2
Summary of mire and catchment level data. The spatial resolution provided when relevant.

Index	Description	Resolution [m]	Source
Mire and catchment geography			
Age [years BP]	Mean catchment age	2 × 2	DEM ^a (Swedish Mapping, Cadastral and Land Registration Authority) and shore displacement curve (Renberg and Segerström, 1981) ^b
Coast_dist [m]	Shortest distance between the mire polygon and the present coastline		Swedish Mapping, Cadastral and Land Registration Authority ^b
Elevation [m]	Mean mire elevation above sea level	2 × 2	DEM ^a (Swedish Mapping, Cadastral and Land Registration Authority) ^b
Area(mire) [ha]	Mire area	1:10,000	Property map (Swedish Mapping, Cadastral and Land Registration Authority) ^b
Area(UC) [ha]	Unique catchment area		DEM ^a (Swedish Mapping, Cadastral and Land Registration Authority) ^b
Shape	Mire shape index		Property map (Swedish Mapping, Cadastral and Land Registration Authority) ^b
UC/Mire	Areal ratio between the unique catchment and the mire area		DEM ^a and Property ^b map (Swedish Mapping, Cadastral and Land Registration Authority)
UC/TC	Areal ratio between the unique and total catchments.		DEM ^a (Swedish Mapping, Cadastral and Land Registration Authority) ^b
Catchment land use/land cover (unique catchment)			
Arable [%]	Arable land in the catchment	1: 10,000	Property map (Swedish Mapping, Cadastral and Land Registration Authority)
Conifer [%]	Coniferous forest in the catchment	--:--	--:--
Deciduous [%]	Deciduous forest in the catchment	--:--	--:--
Open [%]	Open areas in the catchment	--:--	--:--
Water [%]	Water in the catchment	--:--	--:--
Catchment Quaternary deposits (unique catchment)			
Clay-silt [%]	Clay-silt in the catchment	1:100,000	Quaternary deposits map (Geological Survey of Sweden)
Coarse [%]	Coarse sediments in the catchment	--:--	--:--
Sand [%]	Sand in the catchment	--:--	--:--
Till [%]	Till in the catchment	--:--	--:--
Catchment bedrock (unique catchment)			
Felsic [%]	Felsic bedrock in the catchment	1:50,000	Bedrock map (Geological Survey of Sweden)
Fels.-Interm. [%]	Felsic-intermediate bedrock in the catchment	--:--	--:--
Interm. [%]	Intermediate bedrock in the catchment	--:--	--:--
Mafic [%]	Mafic bedrock in the catchment	--:--	--:--
Mire and catchment topography			
Moisture (Mire)	Median mire topographic wetness index (TWI)	24 × 24	DEM ^a (Swedish Mapping, Cadastral and Land Registration Authority) ^b
Moisture (UC)	Mean catchment soil moisture index	2 × 2	Soil moisture map (Swedish University of Agricultural Sciences)
Slope(Mire) [%]	Mire mean slope	2 × 2	DEM ^a (Swedish Mapping, Cadastral and Land Registration Authority) ^b
Slope(UC) [%]	Mean catchment slope	2 × 2	DEM ^a (Swedish Mapping, Cadastral and Land Registration Authority) ^b
Mire vegetation			
NDVI	Mean mire normalized difference vegetation index	10 × 10	Sentinel-2 Level 2A (European Space Agency) ^b
Vol. [m ³ ha ⁻¹]	Median mire tree standing volume	12.5 × 12.5	SLU Forest Map, Dept. of Forest Resource Management, Swedish University of Agricultural Sciences, Umeå

^a Digital Elevation Model.

^b Indices calculated from the data sources.

with one predictive component and one orthogonal component, to describe structures in the dataset and identify variables that control mire NDVI patterns. We focus on the predictive component, but for visualization and comparability of the models, we show one orthogonal component in all models.

The OPLS model separates variation in the predictive component (x) that is linearly related to the determinant (y) and variation in the predictors (x) that is orthogonal to the determinant (y). The OPLS method identify variables that co-vary with the determinant. These will have high positive or negative loadings on the predictive axis (pq[1]) and, hence, be more positively or negatively correlated with the determinant the further away from the origin they are found. Variables that do not correlate with the predictor add “noise” to the model and will have high loadings on the orthogonal axis (poso[1]). In addition to variable loadings, we calculated the variable importance on projection (VIP) based on the predictive component. The VIP identifies variables that are important for the model. The VIP is normalized, such that variables with VIP values >1 are important (Galindo-Prieto et al., 2014). In the OPLS models, we highlighted variables that were significant according to the VIP scores.

We used the multivariate statistical software SIMCA 17, Umetrics, Umeå (Eriksson et al., 2006), to generate Class-OPLS models for May–September, where open and tree-covered mires were separated as classes. We defined the NDVI as determinant (y) and defined all other variables as predictors (x). In SIMCA, we used the auto-transform

function to identify and transform variables that would approach linearity after log-transformation.

3. Results

3.1. Point level models

The sampling points were located at maximum 329 m from the mire edges, with peat depths between 5 and >300 cm (Table E.3). On average tree-covered and open mires had similar depths and the deepest peat was found in an open area (Depth_{max} ≥ 300 cm). The lateral distance to mineral soil (Edge_dist) was, on average, longer in tree-covered sampling points (Edge_dist_{mean} = 35.7 m) compared to open points (Edge_dist_{mean} = 30.5 m) and the longest distance (Edge_dist_{max} = 329.0 m) was represented by an open sampling point.

The electrical conductivity was 21–145 μS cm⁻¹ and macro-nutrient concentrations: C 411–521 mg g⁻¹ (dw), N 3.9–16.6 mg g⁻¹ (dw), P 0.3–1.4 mg g⁻¹ (dw) and K 0.4–3.7 mg g⁻¹ (dw) for edge- and mid-point samples analyzed with ICP-SFMS (Table E.2). Open and tree-covered sampling points were similar with regards to variation in conductivity and elemental concentrations. We provide a complete overview of the elemental composition (Table E.2) and peat physical properties (Table E.3) in Supporting information.

Point level OPLS models

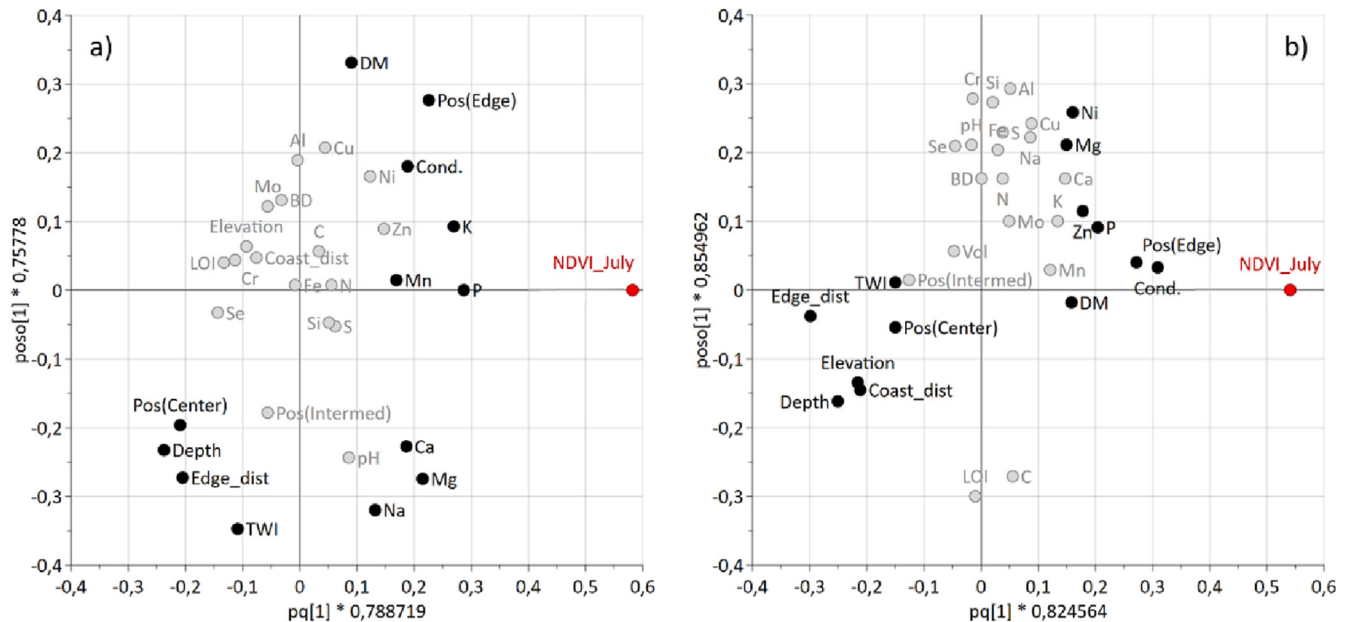


Fig. 4. OPLS results for open (a) and tree-covered (b) points during peak season. Variables marked in black are significant for the July NDVI models and variables in gray are non-significant according to the predictive VIP scores (variable importance on projection).

In open mire points, the peak season model had the highest R^2Y_{cum} (0.56), i.e. the proportion variance in y (NDVI) that is explained by the model. We could describe 50–56 % of the variation in NDVI for open points ($N = 46$) and 47–56 % of the variation in NDVI for tree-covered points ($N = 89$) using monthly OPLS models (Table E.4). When tree-covered and open points were pooled ($N = 135$), we could describe 43–49 % of the total variation in NDVI. The orthogonal components were significant in all models for tree-covered points, while they were non-significant for open points at $p < 0.05$. For models including both tree-covered and open mire points, the orthogonal components were significant in all months except for the May model.

The OPLS model results for open and tree-covered points were similar throughout the vegetation period (Table E.4, and Fig. E.2). Variables that describe proximity to mineral soil, i.e. distance to mire edge (*Edge_dist*), peat depth (*Depth*) and points by the center of the mire transect (*pos(center)*), were negatively correlated with NDVI (Fig. 4). Mire age, as described using mire elevation (*Elevation*) was negatively correlated with NDVI in all models for tree-covered points and in the June model for open points. In addition, the wetness by the sampling point (*TWI*) was negatively correlated to NDVI, and significant according to the predictive VIP score, during all months for tree-covered points and in the May and September models for open points.

Sampling points at mire edges (*pos(edge)*) and conductivity (*Cond.*) were positively correlated with NDVI in all models. In addition, different combinations of dry matter content (*DM*) and phosphorus (*P*), potassium (*K*), nickel (*Ni*), magnesium (*Mg*), manganese (*Mn*) and zinc (*Zn*) were positively correlated with NDVI in the open and tree-covered models, depending on month. The tree-standing volume was not significant for NDVI in any of the point level models.

3.2. Mire level models

Sampled open mires were, on average, larger and moister, with lower slopes, compared to tree-covered mires (Table E.5). Catchments associated with open mires were larger and drier compared to catchments of tree-covered mires, while the catchment-to-mire area ratios were lower in open compared to tree-covered mires. Felsic-intermediate bedrock, till soil and coniferous forest dominated catchments associated both with

tree-covered and open mires. Throughout the vegetation period, the NDVI of tree-covered mires was higher compared to open mires (Table E.5).

The model could describe 71–82 % of the variation in NDVI in the tree-covered sampled mires ($N = 22$; Table E.7). For open mires ($N = 25$), the model performed well in early and mid-season (May $R^2Y_{Cum} = 71$ %, June $R^2Y_{Cum} = 61$ %, July $R^2Y_{Cum} = 63$ %), with decreasing R^2Y_{Cum} towards the end of the vegetation period. In August, we could describe 49 % and in September 46 % of the variation in NDVI. In the OPLS models including both tree-covered and open mires ($N = 47$), we could describe 54–68 % of the variation in NDVI, with the highest R^2Y_{Cum} in September. The orthogonal components were significant in all models for the tree-covered mires, while only the May model for open mires and the May and September models for all mires were significant at $p < 0.05$.

Variables describing mire and landscape age, i.e. mean catchment age (*Age*), mire elevation (*Elevation*) and mire distance to coast (*Coast_dist*), were significant and negatively correlated to NDVI in all models except September for open mires and all models except May and July for tree-covered mires (Figs. 5 and E.3), according to their predictive VIP scores. In addition, mire (*Area(mire)*) and catchment (*Area(UC)*) areas were negatively correlated with NDVI in all models except for the June model for open mires, where only catchment area was significantly correlated to NDVI. The catchment-to-mire ratio (*UC/mire*) was positively correlated to NDVI in tree-covered mires. In open mires, mire (*Moisture(mire)*) and catchment moisture (*Moisture(UC)*) were negatively correlated with NDVI during green-up and senescence. In open mires, the NDVI was positively correlated to mire slope (*Slope(mire)*) during green-up and senescence and positively correlated to catchment slope (*Slope(UC)*) in May–July and September. Finally, mire shape (*Shape*) was negatively correlated with NDVI in all tree-covered mire models as well as in the July–September models for open mires. Importantly, in tree-covered mires, the dominating driver of NDVI in all models was the tree-standing volume, which was positively correlated to the NDVI.

3.3. Landscape level models

When we scaled up from the sampled mires at the mire level to all pristine and moderately drained mires at the landscape level, open mires were still, on average, larger and less sloping compared to tree-covered mires

Mire level OPLS models

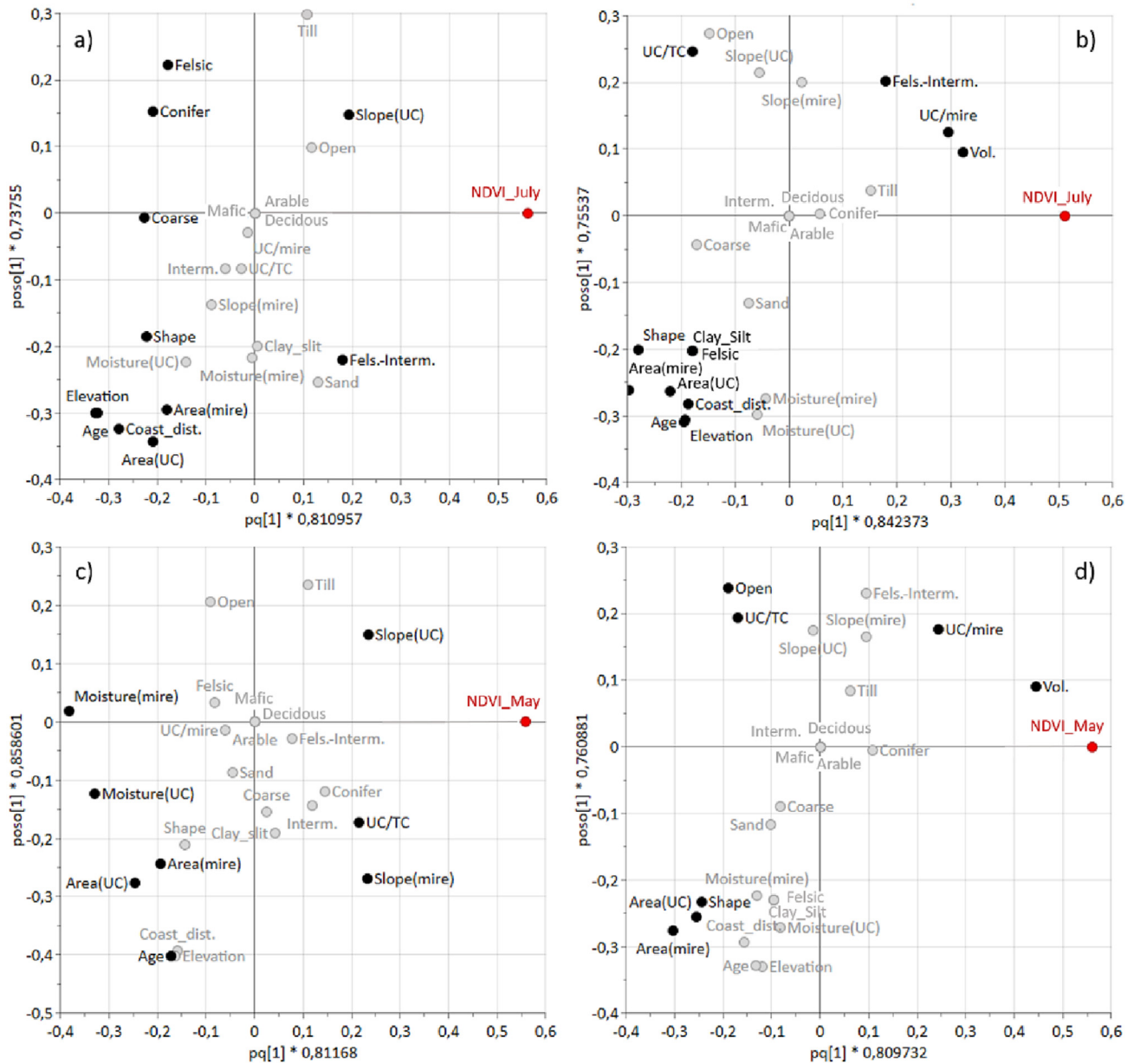


Fig. 5. Mire level OPLS results for open (a) and tree-covered (b) mires during green up as well as for open (c) and tree-covered (d) mires during peak season. Variables marked in black are significant and variables in gray are non-significant according to the predictive VIP scores (variable importance on projection).

(Table E.8). Catchment areas for open mires were larger and moister compared to tree-covered mires, while catchment slopes were similar for open and tree-covered. Similar to the sampled mires, felsic-intermediate bedrock, till soil and coniferous forest dominated both tree-covered and open catchments at the landscape level. Throughout the vegetation period, the NDVI of tree-covered mires was higher compared to open mires (Table E.8).

At the landscape level, we could describe 23–40 % of the variation in NDVI on open mires ($N = 330$) and 20–35 % of the variation in NDVI on tree-covered mires ($N = 1246$; Table E.9). When all mires were included ($N = 1576$), we could describe 36–49 % of the variation in NDVI, depending on month. For open mires, the September OPLS model had the highest R^2 YCum score (0.40) and for tree-covered mires the May model scored highest (0.35). All models had significant predictive and orthogonal components ($p < 0.05$).

In the June–September models for open mires and in the June and July models for tree-covered mires we found a significant negative correlation

between indices describing mire and catchment age (Age, Elevation and Coast_dist) and NDVI according to the predictive VIP scores (Figs. 6 and E.4). In the May model for open mires, there was instead a positive correlation between the age indices and mire NDVI. In open mires, catchment moisture (Moisture(UC)) was negatively correlated to NDVI throughout the entire vegetation period. Similar to the mire level models for sampled mires, mire and catchment areas (Area(mire) and Area(UC)) as well as mire shape (Shape) were negatively correlated with NDVI in tree-covered mires. In several of the models, percentages of open areas (Open), water (Water) and coarse sediments (Coarse) in the catchment area were negatively correlated with NDVI.

The catchment-to-mire ratio (UC/mire) was positively correlated to NDVI in all landscape level models apart from the May model for open mires. Similar to the mire level models, the tree standing volume dominated the landscape OPLS models for tree-covered mires. In open mires, mire slope was positively correlated with NDVI in the August and

Landscape level OPLS models

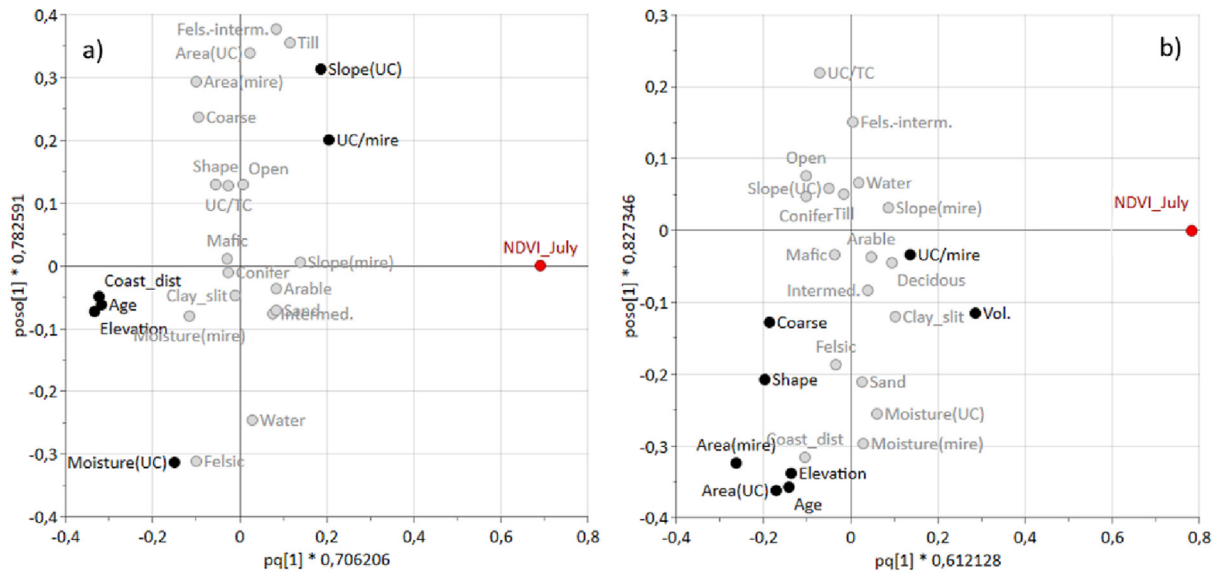


Fig. 6. Landscape level OPLS results for open (a) and tree-covered (b) mires during peak season. Variables marked in black are significant and variables in gray are non-significant according to the VIP scores (variable importance on projection).

September models and catchment slopes in all models except for the May model. Aside from these, the percentages of coniferous forest (Conifer), till (Till) and felsic-intermediate (fels.-interm.) bedrock in the catchment correlated positively with NDVI in some of the open mire models at the landscape level (Fig. E.4).

3.4. Uncertainties in satellite NDVI products

At the larger spatial scales (i.e. mire and landscape levels), the tree standing volume totally dominated the NDVI signal in tree-covered mires regardless of studied month (Figs. 56 and E.3–E.4). Hence, in tree-covered mires the NDVI describes catchment driven canopy patterns rather than mire surface vegetation patterns. Interestingly, and in contrast to NDVI patterns at the mire level (Figs. 5–6, E.3–E.4), the tree standing volume was not a predominant driver of NDVI at the sampling point level (Figs. 4 and E.2). This could simply reflect differences in spatial resolutions between the NDVI (10 × 10 m) and the tree standing volume grids (12.5 × 12.5 m), as well as the representability of the sampling points within the pixels. Moreover, we combined measured peat properties (6 × 6 × 10 cm peat sample) with terrain indices at diverse spatial scales (2 × 2 m to 24 × 24; Table 2) based on different remote sensing techniques. Differences in spatial resolutions naturally resulted in uncertainties in our model input data.

Given the various spatial resolutions, the predictive models that we generated on sampling point and mire levels were very strong (R^2 YCum up to 0.8, Table E.4 and Table E.7) and we could confidently interpret the model outcomes. As we scaled up from the sampled mires to the entire landscape, our predictive models had a considerably lower degree of explanation (Table E.9). Nevertheless, the catchment responses and indications of oligotrophication were preserved during peak season (Fig. E.4) and must, hence, be robust at the landscape level at least during parts of the vegetation period. We might not be able to generate stronger predictive models at the landscape level without considering within-mire variation in vegetation patterns and sub-catchments responses on local mire NDVI patterns. Further, structural vegetation properties would likely add valuable information on nutrient driven vegetation patterns (Räsänen et al., 2020), aside from the spectral properties we applied in this study. These are important considerations for future studies on catchment driven mire vegetation patterns.

4. Discussion

4.1. Mire NDVI as a function of peat nutrient concentrations

It is widely established that the mire nutrient regime, in particular the availability of nitrogen, phosphorus and potassium, are essential for mire plant species composition and productivity in high-latitude landscapes (Bragazza et al., 2005; Økland et al., 2001). The observed co-variation between mire NDVI and several plant nutrient concentrations in the surface peat, especially in open mire parts (Figs. 4 and E.2), confirmed our hypothesis that variation in the mire nutrient regime would be reflected in mire vegetation patterns. This further infers that we, by using the NDVI, can describe how mire vegetation patterns relate to mineral nutrients released by weathering in the surrounding and underlying mineral soils, and transported to the mire surface through surface or groundwater flow paths. This is an important contribution to the general understanding and applicability of the NDVI as a proxy for mire plant productivity at the larger catchment scale.

We based our results on total element concentrations in the solid peat phase. As a long-term archive of the catchment nutrient support to the mire surface, the solid peat phase is more constant and representative compared to, for example, pore water samples from single sampling occasions (Chambers and Charman, 2004). Still, peat nutrient concentrations may reflect the current plant available nutrient pool to different degrees depending on the element and its geochemistry. For example, peat phosphorus is mainly bound to iron or aluminum oxides or hydroxides, in its inorganic (Bloom, 1981; Cuttle, 1983) or organic phosphorus forms (Kooijman et al., 2020). If iron and aluminum concentrations are high, they may represent a considerable sink and limit the plant available phosphorus both in the mire (Kooijman et al., 2020; Richardson, 1985) and in the upland areas (Giesler et al., 2002; Vincent et al., 2012). We found total peat phosphorus concentrations to be positively, although only weakly, correlated to iron and/or aluminum concentrations in the peat (Fig. E.1). Yet, despite this geochemical phosphorus sink, peat phosphorus concentration was excellent in predicting NDVI in open mires, with almost no variation on the orthogonal OPLS-axis, representing variation not related to the response variable (NDVI; Fig. 4). This is likely because mire plants momentarily take up phosphorus that is released from the inaccessible peat pool (Bombonato et al., 2010; Kellogg and Bridgman, 2003), which preserves the strong signal between the catchment phosphorus support and the mire NDVI.

Together with phosphorus, potassium was the element that contributed strongest to the NDVI prediction over the vegetation period, especially in open mire parts (Table E.4). Potassium is likely one of the most mobile nutrients associated with peat, since it is primarily and comparably weakly bound to the cation exchange complex, together with elements such as magnesium and calcium (McCarter et al., 2021). In addition, these elements may be temporarily found in non-crystalline phases before released to the plant available pool (van der Heijden et al., 2017). Based on its mobility, concentrations of potassium reported here should reflect the plant available potassium pool well and, consequently, the co-variation between potassium and NDVI is a vegetation response to more nutrient-rich conditions. In contrast, practically all peat nitrogen is present as organic nitrogen in polymers, thus largely unavailable to plants (Worrall et al., 2022). This explains why we did not find a strong signal between total peat nitrogen concentrations and NDVI (Fig. E.2). Nitrogen fixing *Sphagnum* mosses might also have altered the relation between surface peat nitrogen concentrations and NDVI, to different degrees in opposing parts of the chronosequence. Nitrogen fixation is high in young mires, rich in weathering based mineral nutrients, but can be almost negligible in older mires with the least access to weathering-derived nutrients (Larmola et al., 2014). Based on our results, we cannot infer if nitrogen gradients across the chronosequence have contributed to the observed NDVI patterns. However, while total nitrogen concentrations do not represent plant available nitrogen in peat, studies in upland areas have shown that nitrogen availability can covary with concentrations of calcium, magnesium and phosphorus (Giesler et al., 1998). In our case, such co-variation would strengthen the case of nutrient driven NDVI patterns.

4.2. Edge effects on internal mire nutrient transport

We found higher NDVI by the mire edges compared to mire centers, which describes an internal mire margin-expanse gradient in vegetation patterns (Fig. 4), typical of boreal fens (Korpela and Reinikainen, 1996). In tree-covered mire parts, edges represent shallower peat depths with higher nutrient availability (Hughes and Barber, 2004) and better physical root support from the underlying mineral soil. In addition, mire margins in the studied minerogenic mires are often drier compared to mire centers and, thus, more favorable for tree roots (Bhatti et al., 2006). A higher canopy cover by the edges is probably the main driver of the edge effect on NDVI in tree-covered mire parts. However, we found higher NDVI also in open mire edges compared to open mire expanses, which we interpret as a direct effect of higher nutrient support by the edges from upland lateral flow paths, together with biotic and abiotic immobilization of plant nutrients by the mire margins (Korpela and Reinikainen, 1996). Sampling points at intermediate positions (Fig. 1) were more similar to the central points than edge points (Fig. 4). This suggests that nutrients from the catchment area are effectively immobilized by plants along the edges, and prevented from advancing and supporting plant productivity further out in the mire expanse.

We found further support for nutrient gradients across the mire surface at the mire level. Mire slope correlated positively and mire moisture negatively with NDVI during green-up (May–June) and senescence (September, Figs. E.3–E.4). Depending on the direction of the mire slope, a steep slope might result in lower nutrient retention in the edges and higher nutrient transport from the mire margin to the expanse, leading to more even nutrient distributions and, consequently, more even mire vegetation patterns across the mire surface (Damman, 1986; Laroque et al., 2016; Rehell et al., 2019). We interpret the negative co-variation between mire moisture and NDVI as a result of inundation, such that the mire vegetation is less constrained by wet surface conditions and exposed earlier after spring and autumn floods in steep sloping mires (Jabłońska et al., 2011), thus, enabling higher mire productivity sooner after a flooding event (Balliston and Price, 2022). In addition, a wetter mire surface might result in dilution of elements, with lower concentrations of plant available nutrients (Ågren et al., 2012; Eppinga et al., 2010).

According to the mire margin-expanse gradient, a larger mire area should result in weaker edge effects on NDVI as the relative importance of the edges on the total mire area decreases. This was apparent across all

sampled mires and months, and in tree-covered mires at the larger landscape level (Figs. E.3–E.4). At the same time, a more complex mire shape, often associated with the larger mires, should result in stronger edge effects on NDVI, as the contact area between mires and the surrounding catchments increases with more complex shapes (Rehell et al., 2019). However, here we found a negative correlation between mire shape and NDVI during several of the studied months, both for open and tree-covered mires and at the mire and landscape levels (Figs. E.3–E.4). In the chronosequence, old mire complexes represent the most complex mire shapes (unpublished data). Hence, in the study area, mire shape must be understood and interpreted as a function of mire lateral expansion over the Holocene. In this way, the negative co-variation between the mire shape and NDVI has stronger association with the aging of the mire landscape than to edge effects across catchments of similar ages.

4.3. Catchment eco-hydrological settings as drivers of mire NDVI

We found strong indications that mire productivity, as described using the NDVI, depends on the proximity to the contributing catchment area (Figs. 4 and E.2). As peat accumulates and the mire surface progressively becomes disconnected from the mineral soil (both vertically and laterally), mire plants receive less nutrients from weathering products (Hughes and Barber, 2004), still though receiving water from the surrounding catchment. In our study, this resulted in a lower mire NDVI (Figs. 4 and E.2). The importance of the contributing upslope catchment area on mire NDVI was also preserved when we scaled up from the sampling points to the mire level using remotely sensed data only (Figs. 5–6 and E.3–E.4), supporting this conclusion.

In mires at the landscape level, and in the tree-covered sampled mires, a larger catchment area relative to the recipient mire resulted in higher mire NDVI, suggesting a stronger nutrient support from upland mineral soils. Catchment eco-hydrological settings, in particular catchment slope and wetness were additional important drivers of open mire NDVI (Figs. E.3–E.4). In this context, a steep catchment slope suggests more incoming plant nutrients from the catchment compared to a flatter catchment where dissolved nutrients might be retained in stagnant water, prevented from traveling downslope the catchment (Autio et al., 2020; Kortelainen et al., 2006). In the chronosequence, especially in the older parts, flat, moist catchments may be comprised of shallow peat soil (Ågren et al., 2022). Here, nutrients and weathering products are more likely to be immobilized if plant nutrients are taken up by the living plants and stored as peat (Foster and Bhatti, 2005; Prescott et al., 2000). On the other hand, a very steep catchment might result in shorter contact time between the soil water and mineral soil, resulting in more nutrient-poor minerogenic water reaching the mire (Maher, 2010).

Aside from topography, catchment mineralogy is crucial for the nutrient input to mires, as weathering products and other particulate and dissolved nutrients depend on the contact between mineral soil and the topographically driven runoff (Kharanzhevskaya et al., 2020). The positive correlation between felsic-intermediate bedrock and NDVI, both in open and tree-covered mires (Figs. E.3–E.4), could reflect the fertilizing effect that mica schist has on mire vegetation, especially as a source of potassium (Brady et al., 2008). Unfortunately, there is no detailed information on which minerals in the bedrock class that are present in our study area. During several months, NDVI was lower in mires with catchments high in felsic bedrock and/or coarse sediments. Both of these represent sources of low nutrient supply to mires; felsic bedrock due to its low weatherability and coarse sediments due to the low capacity to adsorb and release nutrients compared to finer textured sediments (Brady et al., 2008).

4.4. The role of landscape aging on mire NDVI

We found clear landscape age effects on NDVI, with less productive mires in the older parts of the chronosequence. Based on the consistent negative correlation between NDVI and peat depth, as well as between NDVI and the horizontal distance to mire edge (Figs. 4 and E.2), we argue that

long-term peat accumulation must have caused succession towards more oligotrophic mire surface conditions over time, despite still receiving water from the supporting catchment. Furthermore, our analyses at the larger spatial scales (mire and landscape levels) strengthened the hypothesis that mire NDVI is controlled by Holocene landscape aging, since both direct and indirect indices describing mire age co-varied with NDVI (Figs. 5–6 and E.3–E.4).

Easily weatherable minerals may form strong nutrient gradients across aging landscapes and control the transport of nutrients to mires (Starr and Lindroos, 2006). In the study area, potassium and calcium rich biotite and hornblende are present in the youngest part of the chronosequence (<2000 years), while these have completely weathered from the uppermost soil layers in older parts of the chronosequence (Hoffland et al., 2002). When the easily weathered minerals disappear, fungal hyphae may start to tunnel feldspar grains, which results in further, slower, release of potassium and calcium to biota (Hoffland et al., 2002). When it comes to phosphorus, apatite is the main source (Mehmood et al., 2018). Within ~500 years after exposure, all phosphate from apatite may be weathered from the mineral surface soil in the upland areas (Giesler, 2010), and even within only ~25 years under acidic mires conditions (Le Roux et al., 2006). Thus, in young soils, phosphorus export from apatite weathering to mires can potentially be large depending on local topography. Over time, the phosphorus transport to downslope located mires gradually slows down as the weathering rate decreases and the released phosphorus is reallocated to organic matter or sorbed in the podzol B-horizon (Tuyishime et al., 2022; Wallander and Thelin, 2008; Wood et al., 1984). Similarly, nitrogen leaching from upland soils is more likely in the younger stages of mire development and will rapidly decline as nitrogen is retained in upland soils as organic nitrogen (Blaško et al., 2015). In addition, high phosphorus and potassium concentrations support the potential for nitrogen fixation, particularly in younger mires.

Based on our results, we cannot judge if disconnection from mineral soil due to peat increment alone resulted in the observed lowering of NDVI in older mires, or if mire NDVI in addition is suppressed due to nutrient-poorer lateral water inflows in older parts of the chronosequence. Given the various mineral weathering rates in different parts of the chronosequence, though, it is very likely that oligotrophication of the mire surface is a combined response to the two processes. Based on the observed covariation between NDVI and phosphorus and potassium it is likely that the chronosequence mires are influenced by, at least, three long-term nutrient gradients: 1) a nitrogen gradient formed by nitrogen fixing bacteria in Sphagnum mosses, 2) potassium and calcium gradients formed from biotite, hornblende and feldspar weathering and 3) a phosphorus gradient formed from apatite weathering and decreased leaching losses. The relative importance of the individual gradients remains to be explored.

4.5. Implications of catchment land use on mire vegetation patterns

Our results and interpretations, covering 5000 years of landscape evolution, contribute beyond the limits of the studied chronosequence, to the understanding of how a continuous supply of nutrients from the underlying and upslope area regulate mire vegetation patterns. By further extension, our results illustrate how the surrounding landscape controls fundamental mire ecosystem services. The importance of the catchment control on mire vegetation patterns inevitably lead to the question how land-use in the upslope catchment area disturb mires hydrologically and biogeochemically through changed hydrological connectivity between mineral soil and peat. Efforts to explain mire hydrological disturbance have often been focused to drained or otherwise exploited peatlands (McCarter et al., 2021; Nieminen et al., 2022), while the magnitude of anthropogenic mire disturbance from land-use in the upslope forested catchment area causing, for example oligotrophication (Tahvanainen, 2011), is limited to single mires. If forest management practices in the catchment area prevent nutrients from reaching downslope mires (Finér et al., 2021) or if the practices alter mire hydrology so that the mire surface becomes drier, the mire nutrient balance can be disturbed (Nwaishi et al., 2022). In addition, a drier

mire surface may favor shrubs over mosses (Churchill et al., 2015; Park et al., 2016), depending on the resilience of the mire vegetation (Piilo et al., 2023). Finally, weathering rates of boreal forest soils have gained increased interest recently due to nutrient depletion after forest harvesting (Akselsson et al., 2019; Klaminder et al., 2011). If weathering rates cannot meet the demands of the upland vegetation after nutrients have been recycled at site (Akselsson et al., 2019), downslope freshwater systems, including mires, might suffer from effects of forestry-caused nutrient depletion (Huser et al., 2018). Based on this, we suggest that questions focusing on large-scale land-use (changes) in the upslope catchment area and their effects on mire nutrient regime, such as mire oligotrophication, are important to consider in future studies.

CRediT authorship contribution statement

Betty Ehnvall, Anneli M. Ågren, Mats B. Nilsson, Matthias Peichl, William Lidberg and Mats G. Öquist conceptualized the study and designed the methodology. Betty Ehnvall, William Lidberg, Koffi Dodji Noumonvi, Reiner Giesler and Carl-Magnus Mörth gathered the data. Betty Ehnvall performed the analyses and wrote the first draft. All authors interpreted and discussed the ideas and results, and contributed to writing the final manuscript.

Data availability

Scripts and data can be accessed from the project GitHub page (https://github.com/BettyEhnvall/Mire_chronosequence).

Declaration of competing interest

The authors have no conflicts of interest to declare.

Acknowledgements

This work was primarily funded by the Swedish Research Council Formas [2016-00896], [2020-01436], [2020-00028] and [2021-00115], with support from the Swedish Nuclear Fuel and Waste Management Company (SKB). This work was partially supported by the Wallenberg AI, Autonomous Systems and Software Program – Humanities and Society (WASP-HS) funded by the Marianne and Marcus Wallenberg Foundation and the Marcus and Amalia Wallenberg Foundation. In addition, Knut and Alice Wallenberg Foundation [2018.0259] supported the work. The authors would like to thank André Wästlund and Michaela Lundberg for initial discussions on NDVI extraction, as well as Anders Löfgren (SKB) for interesting discussions on mire development. The authors have no conflicts of interest to declare.

Appendix A. Supplementary data

Supplementary data to this article can be found online at <https://doi.org/10.1016/j.scitotenv.2023.165132>.

References

- Ågren, A.M., Haei, M., Blomkvist, P., Nilsson, M.B., Laudon, H., 2012. Soil frost enhances stream dissolved organic carbon concentrations during episodic spring snow melt from boreal mires. *Glob. Chang. Biol.* 18, 1895–1903. <https://doi.org/10.1111/j.1365-2486.2012.02666.x>.
- Ågren, A.M., Larson, J., Paul, S.S., Laudon, H., Lidberg, W., 2021. Use of multiple LIDAR-derived digital terrain indices and machine learning for high-resolution national-scale soil moisture mapping of the Swedish forest landscape. *Geoderma* 404, 115280. <https://doi.org/10.1016/j.geoderma.2021.115280>.
- Ågren, A.M., Hasselquist, E.M., Stendahl, J., Nilsson, M.B., Paul, S.S., 2022. Delineating the distribution of mineral and peat soils at the landscape scale in northern boreal regions. *EGU sphere* 1–23. <https://doi.org/10.5194/egusphere-2022-79>.
- Akselsson, C., Belyazid, S., Stendahl, J., Finlay, R., Olsson, B.A., Eriandsson Lampa, M., Wallander, H., Gustafsson, J.P., Bishop, K., 2019. Weathering rates in Swedish forest soils. *Biogeosciences* 16, 4429–4450. <https://doi.org/10.5194/bg-16-4429-2019>.
- Anderson, T.G., Christie, D.A., Chávez, R.O., Olea, M., Anchukaitis, K.J., 2021. Spatiotemporal peatland productivity and climate relationships across the western south American Altiplano. *J. Geophys. Res. Biogeosci.* 126, e2020JG005994. <https://doi.org/10.1029/2020JG005994>.

- Antala, M., Juszczak, R., van der Tol, C., Rastogi, A., 2022. Impact of climate change-induced alterations in peatland vegetation phenology and composition on carbon balance. *Sci. Total Environ.* 827, 154294. <https://doi.org/10.1016/j.scitotenv.2022.154294>.
- Autio, A., Ala-Aho, P., Ronkanen, A.-K., Rossi, P.M., Kløve, B., 2020. Implications of peat soil conceptualization for groundwater exfiltration in numerical modeling: a study on a hypothetical peatland hillslope. *Water Resour. Res.* 56, e2019WR026203. <https://doi.org/10.1029/2019WR026203>.
- Avetov, N.A., Kuznetsov, O.L., Shishkonakova, E.A., 2021. Soils of oligomesotrophic and mesotrophic bogs in the boreal zone of West Siberia: possibilities of molecular diagnostics within the framework of the type of mesotrophic peat soils. *Eurasian Soil Sci.* 54, 689–701. <https://doi.org/10.1134/S1064229321030029>.
- Balliston, N., Price, J.S., 2022. Beyond fill and spill: hydrological connectivity in a sub-arctic bog-fen-tributary complex in the Hudson Bay Lowlands, Canada. *Hydrol. Process.* 36, e14575. <https://doi.org/10.1002/hyp.14575>.
- Beven, K.J., Kirkby, M.J., 1979. A physically based, variable contributing area model of basin hydrology/Un modèle à base physique de zone d'appel variable de l'hydrologie du bassin versant. *Hydrol. Sci. Bull.* 24, 43–69. <https://doi.org/10.1080/02626667909491834>.
- Bhatti, J.S., Errington, R.C., Bauer, I.E., Hurdle, P.A., 2006. Carbon stock trends along forested peatland margins in central Saskatchewan. *Can. J. Soil Sci.* 86, 321–333. <https://doi.org/10.4141/S05-085>.
- Blaško, R., Holm Bach, L., Yarwood, S.A., Trumbore, S.E., Högborg, P., Högborg, M.O., 2015. Shifts in soil microbial community structure, nitrogen cycling and the concomitant declining N availability in ageing primary boreal forest ecosystems. *Soil Biol. Biochem.* 91, 200–211. <https://doi.org/10.1016/j.soilbio.2015.08.041>.
- Bloom, P.R., 1981. Phosphorus adsorption by an aluminum-peat complex. *Soil Sci. Soc. Am. J.* 45, 267–272. <https://doi.org/10.2136/sssaj1981.03615995004500020008x>.
- Boelman, N.T., Stieglitz, M., Rueth, H.M., Sommerkorn, M., Griffin, K.L., Shaver, G.R., Gamon, J.A., 2003. Response of NDVI, biomass, and ecosystem gas exchange to long-term warming and fertilization in wet sedge tundra. *Oecologia* 135, 414–421. <https://doi.org/10.1007/s00442-003-1198-3>.
- Bombonato, L., Siffi, C., Gerdol, R., 2010. Variations in the foliar nutrient content of mire plants: effects of growth-form based grouping and habitat. *Plant Ecol.* 211, 235–251. <https://doi.org/10.1007/s11258-010-9786-x>.
- Brady, N.C., Weil, R.R., Weil, R.R., 2008. *The Nature and Properties of Soils*. vol. 13. Prentice Hall, Upper Saddle River, NJ, pp. 662–710.
- Bragazza, L., Rydin, H., Gerdol, R., 2005. Multiple gradients in mire vegetation: a comparison of a Swedish and an Italian bog. *Plant Ecol.* 177, 223–236.
- Bring, A., Thorslund, J., Rosén, L., Tonderski, K., Åberg, C., Envall, I., Laudon, H., 2022. Effects on groundwater storage of restoring, constructing or draining wetlands in temperate and boreal climates: a systematic review. *Environ. Evid.* 11, 38. <https://doi.org/10.1186/s13750-022-00289-5>.
- Chambers, F.M., Charman, D.J., 2004. Holocene environmental change: contributions from the peatland archive. *The Holocene* 14, 1–6. <https://doi.org/10.1191/0959683604hl684ed>.
- Churchill, A.C., Turetsky, M.R., McGuire, A.D., Hollingsworth, T.N., 2015. Response of plant community structure and primary productivity to experimental drought and flooding in an Alaskan fen. *Can. J. For. Res.* 45, 185–193. <https://doi.org/10.1139/cjfr-2014-0100>.
- Cohen, M.J., Creed, I.F., Alexander, L., Basu, N.B., Calhoun, A.J.K., Craft, C., D'Amico, E., DeKeyser, E., Fowler, L., Golden, H.E., Jawitz, J.W., Kalla, P., Kirkman, L.K., Lane, C.R., Lang, M., Leibowitz, S.G., Lewis, D.B., Marton, J., McLaughlin, D.L., Mushet, D.M., Raanan-Kiperwas, H., Rains, M.C., Smith, L., Walls, S.C., 2016. Do geographically isolated wetlands influence landscape functions? *Proc. Natl. Acad. Sci. U. S. A.* 113, 1978–1986. <https://doi.org/10.1073/pnas.1512650113>.
- Conrad, O., Bechtel, B., Bock, M., Dietrich, H., Fischer, E., Gerlitz, L., Wehberg, J., Wichmann, V., Böhner, J., 2015. System for automated geoscientific analyses (SAGA) v. 2.1.4. *Geosci. Model Dev.* 8, 1991–2007. <https://doi.org/10.5194/gmd-8-1991-2015>.
- Crichton, K.A., Anderson, K., Charman, D.J., Gallego-Sala, A., 2022. Seasonal climate drivers of peak NDVI in a series of Arctic peatlands. *Sci. Total Environ.* 838, 156419. <https://doi.org/10.1016/j.scitotenv.2022.156419>.
- Cuttle, S.P., 1983. Chemical properties of upland peats influencing the retention of phosphate and potassium ions. *J. Soil Sci.* 34, 75–82. <https://doi.org/10.1111/j.1365-2389.1983.tb00814.x>.
- Damman, A.W.H., 1986. Hydrology, development, and biogeochemistry of ombrogenous peat bogs with special reference to nutrient relocation in a western Newfoundland bog. *Can. J. Bot.* 64, 384–394. <https://doi.org/10.1139/b86-055>.
- Diamond, J.S., Epstein, J.M., Cohen, M.J., McLaughlin, D.L., Hsueh, Y.-H., Keim, R.F., Duberstein, J.A., 2021. A little relief: ecological functions and autogenesis of wetland microtopography. *Wiley Interdiscip. Rev. Water* 8, e1493. <https://doi.org/10.1002/wat2.1493>.
- Ecke, F., Rydin, H., 2000. Succession on a land uplift coast in relation to plant strategy theory. *Ann. Bot. Fenn.* 37, 163–171.
- Ehrvall, B., Ratcliffe, J.L., Bohlin, E., Nilsson, M.B., Öquist, M.G., Sponseller, R.A., Grabs, T., 2023. Landscape constraints on mire lateral expansion. *Quat. Sci. Rev.* 302, 107961. <https://doi.org/10.1016/j.quascirev.2023.107961>.
- Eklundh, L., Jin, H., Schubert, P., Guzinski, R., Heliasz, M., 2011. An optical sensor network for vegetation phenology monitoring and satellite data calibration. *Sensors* 11, 7678–7709. <https://doi.org/10.3390/s110807678>.
- Eppinga, M.B., Rietkerk, M., Belyea, L.R., Nilsson, M.B., Rüter, P.C.D., Wassen, M.J., 2010. Resource contrast in patterned peatlands increases along a climatic gradient. *Ecology* 91, 2344–2355. <https://doi.org/10.1890/09-1313.1>.
- Eriksson, L., Kettaneh-Wold, N., Trygg, J., Wikström, C., Wold, S., 2006. *Multi- and Megavariate Data Analysis: Part I: Basic Principles and Applications*. Umetrics Inc.
- Fergus, Carol Emi, Jean-François, Lapierre, Oliver, Samantha K., Skaff, Nicholas K., Cheruvellil, Kendra S., Katherine, Webster, Caren, Scott, Patricia, Soranno, 2017. The freshwater landscape: lake, wetland, and stream abundance and connectivity at macro-scales. *Ecosphere* 8, e01911. <https://doi.org/10.1002/ecs2.1911>.
- Finér, L., Lepistö, A., Karlsson, K., Räike, A., Härkönen, L., Huttunen, M., Joensuu, S., Kortelainen, P., Mattsson, T., Piirainen, S., Sallantausta, T., Sarkkola, S., Tattari, S., Ukonmaanaho, L., 2021. Drainage for forestry increases N, P and TOC export to boreal surface waters. *Sci. Total Environ.* 762, 144098. <https://doi.org/10.1016/j.scitotenv.2020.144098>.
- Forman, R.T.T., Gordon, M., 1986. *Landscape Ecology*. John Wiley & Sons.
- Foster, N., Bhatti, J., 2005. Forest ecosystems: nutrient cycling. *Encyclopedia of Soil Science*, Second edition CRC Press <https://doi.org/10.1201/NOE0849338304.ch145>.
- Galindo-Prieto, B., Eriksson, L., Trygg, J., 2014. Variable influence on projection (VIP) for orthogonal projections to latent structures (OPLS). *J. Chemom.* 28, 623–632. <https://doi.org/10.1002/cem.2627>.
- Giesler, 2010. Rapid transformation of P across a podzol chronosequence in Northern Sweden. *Geochim. Cosmochim. Acta* 74, A329.
- Giesler, R., Högborg, M.H., Högborg, P.H., 1998. Soil chemistry and plants in Fennoscandian boreal forests as exemplified by a local gradient. *Ecology* 79 (1), 119–137.
- Giesler, R., Petersson, T., Högborg, P., 2002. Phosphorus limitation in boreal forests: effects of aluminum and iron accumulation in the humus layer. *Ecosystems* 5, 300–314.
- Glaser, P.H., Janssens, J.A., Siegel, D.I., 1990. The response of vegetation to chemical and hydrological gradients in the lost river peatland, northern Minnesota. *J. Ecol.* 78, 1021–1048. <https://doi.org/10.2307/2260950>.
- Gorelick, N., Hancher, M., Dixon, M., Ilyushchenko, S., Thau, D., Moore, R., 2017. Google Earth engine: planetary-scale geospatial analysis for everyone. *Remote Sens. Environ.* 202, 18–27. <https://doi.org/10.1016/j.rse.2017.06.031>.
- Granath, G., Strengbom, J., Rydin, H., 2010. Rapid ecosystem shifts in peatlands: linking plant physiology and succession. *Ecology* 91, 3047–3056. <https://doi.org/10.1890/09-2267.1>.
- Gunnarsson, U., 2005. Global patterns of Sphagnum productivity. *J. Bryol.* 27, 269–279. <https://doi.org/10.1179/174328205X70029>.
- Gunnarsson, U., Löfroth, M., Sandring, S., 2014. *The Swedish Wetland Survey: Compiled Excerpts From the National Final Report, Rapport/Naturvårdsverket*. Swedish Environmental Protection Agency, Stockholm.
- van der Heijden, G., Legout, A., Mareschal, L., Ranger, J., Dambrine, E., 2017. Filling the gap in ca input-output budgets in base-poor forest ecosystems: the contribution of non-crystalline phases evidenced by stable isotopic dilution. *Geochim. Cosmochim. Acta* 209, 135–148. <https://doi.org/10.1016/j.gca.2017.04.018>.
- Helbig, M., Waddington, J.M., Alekseychik, P., Amiro, B., Aurela, M., Barr, A.G., Black, T.A., Carey, S.K., Chen, J., Chi, J., Desai, A.R., Dunn, A., Euskirchen, E.S., Flanagan, L.B., Friborg, T., Garneau, M., Grelle, A., Harder, S., Heliasz, M., Humphreys, E.R., Ikawa, H., Isabelle, P.-E., Iwata, H., Jassal, R., Korkiakoski, M., Kurbatova, J., Kutzbach, L., Lapshina, E., Lindroth, A., Löfvenius, M.O., Lohila, A., Mammarella, I., Marsh, P., Moore, P.A., Maximov, T., Nadeau, D.F., Nicholls, E.M., Nilsson, M.B., Ohta, T., Peichl, M., Petrone, R.M., Prokushkin, A., Quinton, W.L., Roulet, N., Runkle, B.R.K., Sonntag, O., Strachan, I.B., Taillardat, P., Tuittila, E.-S., Tuovinen, J.-P., Turner, J., Ueyama, M., Varlagin, A., Vesala, T., Wilking, M., Zyrianov, V., Schulze, C., 2020a. The biophysical climate mitigation potential of boreal peatlands during the growing season. *Environ. Res. Lett.* 15, 104004. <https://doi.org/10.1088/1748-9326/abab34>.
- Helbig, M., Waddington, J.M., Alekseychik, P., Amiro, B., Aurela, M., Barr, A.G., Black, T.A., Blanken, P.D., Carey, S.K., Chen, J., Chi, J., Desai, A.R., Dunn, A., Euskirchen, E.S., Flanagan, L.B., Forbrich, I., Friborg, T., Grelle, A., Harder, S., Heliasz, M., Humphreys, E.R., Ikawa, H., Isabelle, P.-E., Iwata, H., Jassal, R., Korkiakoski, M., Kurbatova, J., Kutzbach, L., Lindroth, A., Löfvenius, M.O., Lohila, A., Mammarella, I., Marsh, P., Maximov, T., Melton, J.R., Moore, P.A., Nadeau, D.F., Nicholls, E.M., Nilsson, M.B., Ohta, T., Peichl, M., Petrone, R.M., Petrov, R., Prokushkin, A., Quinton, W.L., Reed, D.E., Roulet, N.T., Runkle, B.R.K., Sonntag, O., Strachan, I.B., Taillardat, P., Tuittila, E.-S., Tuovinen, J.-P., Turner, J., Ueyama, M., Varlagin, A., Wilking, M., Wofsy, S.C., Zyrianov, V., 2020b. Increasing contribution of peatlands to boreal evapotranspiration in a warming climate. *Nat. Clim. Chang.* 10, 555–560. <https://doi.org/10.1038/s41558-020-0763-7>.
- Hoffland, E., Giesler, R., Jongmans, T., van Breemen, N., 2002. Increasing feldspar tunneling by fungi across a north Sweden podzol chronosequence. *Ecosystems* 5, 11–22. <https://doi.org/10.1007/s10021-001-0052-x>.
- Hugelius, G., Loisel, J., Chadburn, S., Jackson, R.B., Jones, M., MacDonald, G., Maruschak, M., Olefeldt, D., Packalen, M., Siewert, M.B., Treat, C., Turetsky, M., Voigt, C., Yu, Z., 2020. Large stocks of peatland carbon and nitrogen are vulnerable to permafrost thaw. *Proc. Natl. Acad. Sci.* 117, 20438–20446. <https://doi.org/10.1073/pnas.1916387117>.
- Hughes, P.D.M., Barber, K.E., 2004. Contrasting pathways to ombrotrophy in three raised bogs from Ireland and Cumbria, England. *The Holocene* 14, 65–77. <https://doi.org/10.1191/0959683604hl690p>.
- Huser, B.J., Futter, M.N., Wang, R., Fölster, J., 2018. Persistent and widespread long-term phosphorus declines in boreal lakes in Sweden. *Sci. Total Environ.* 613–614, 240–249. <https://doi.org/10.1016/j.scitotenv.2017.09.067>.
- Ivanov, K., 1981. *Water Movement in Mirelands*. Academic press Inc., London.
- Jabłońska, E., Pawlikowski, P., Jarzombkowski, F., Chormański, J., Okruszko, T., Kłowski, S., 2011. Importance of water level dynamics for vegetation patterns in a natural percolation mire (Rospuda fen, NE Poland). *Hydrobiologia* 674, 105–117. <https://doi.org/10.1007/s10750-011-0735-z>.
- Järveoja, J., Nilsson, M.B., Gažovič, M., Crill, P.M., Peichl, M., 2018. Partitioning of the net CO₂ exchange using an automated chamber system reveals plant phenology as key control of production and respiration fluxes in a boreal peatland. *Glob. Chang. Biol.* 24, 3436–3451. <https://doi.org/10.1111/gcb.14292>.
- Joosten, H., Clarke, D., 2002. *Wise Use of Mires: Background and Principles Including a Framework for Decision Making*. 304. International Mire Conservation Group. International Peat Society, Jyväskylä, p. 304.
- Kellogg, L.E., Bridgman, S.D., 2003. Phosphorus retention and movement across an ombrotrophic-minerotrophic peatland gradient. *Biogeochemistry* 63, 299–315. <https://doi.org/10.1023/A:1023387019765>.
- Kharanzhevskaya, Yu.A., Voistina, E.S., Sinyutkina, A.A., 2020. Spatial and temporal variations in mire surface water chemistry as a function of geology, atmospheric circulation and zonal features in the south-eastern part of Western Siberia. *Sci. Total Environ.* 733, 139343. <https://doi.org/10.1016/j.scitotenv.2020.139343>.

- Klaminder, J., Lucas, R.W., Futter, M.N., Bishop, K.H., Köhler, S.J., Egnell, G., Laudon, H., 2011. Silicate mineral weathering rate estimates: are they precise enough to be useful when predicting the recovery of nutrient pools after harvesting? *For. Ecol. Manag.* 261, 1–9. <https://doi.org/10.1016/j.foreco.2010.09.040>.
- Kooijman, A.M., Cusell, C., Hedenäs, L., Lamers, L.P.M., Mettrop, I.S., Neijmeijer, T., 2020. Re-assessment of phosphorus availability in fens with varying contents of iron and calcium. *Plant Soil* 447, 219–239. <https://doi.org/10.1007/s11104-019-04241-4>.
- Korpela, L., Reinikainen, A., 1996. A numerical analysis of mire margin forest vegetation in South and Central Finland. *Ann. Bot. Fenn.* 33, 183–197.
- Kortelainen, P., Mattsson, T., Finér, L., Ahtiainen, M., Saukkonen, S., Sallantausta, T., 2006. Controls on the export of C, N, P and Fe from undisturbed boreal catchments, Finland. *Aquat. Sci.* 68, 453–468. <https://doi.org/10.1007/s00027-006-0833-6>.
- Laine, A.M., Juurola, E., Hájek, T., Tuittila, E.-S., 2011. Sphagnum growth and ecophysiology during mire succession. *Oecologia* 167, 1115–1125. <https://doi.org/10.1007/s00442-011-2039-4>.
- Laine, A.M., Lindholm, T., Nilsson, M., Kutznetsov, O., Jassey, V.E.J., Tuittila, E., 2021. Functional diversity and trait composition of vascular plant and *Sphagnum* moss communities during peatland succession across land uplift regions. *J. Ecol.* 109, 1774–1789. <https://doi.org/10.1111/1365-2745.13601>.
- Lane, C.R., Leibowitz, S.G., Autrey, B.C., LeDuc, S.D., Alexander, L.C., 2018. Hydrological, physical, and chemical functions and connectivity of non-floodplain wetlands to downstream waters: a review. *J. Am. Water Resour. Assoc.* 54, 346–371. <https://doi.org/10.1111/1752-1688.12633>.
- Larmola, T., Leppänen, S.M., Tuittila, E.-S., Aarva, M., Merilä, P., Fritze, H., Tiirola, M., 2014. Methanotrophy induces nitrogen fixation during peatland development. *Proc. Natl. Acad. Sci.* 111, 734–739. <https://doi.org/10.1073/pnas.1314284111>.
- Larocque, M., Ferlatte, M., Pellerin, S., Cloutier, V., Munger, J.L., Paniconi, C., Quillet, A., 2016. Chemical and botanical indicators of groundwater inflow to Sphagnum-dominated peatlands. *Ecol. Indic.* 64, 142–151. <https://doi.org/10.1016/j.ecolind.2015.12.012>.
- Larson, J., Lidberg, W., Ågren, A.M., Laudon, H., 2022. Predicting soil moisture conditions across a heterogeneous boreal catchment using terrain indices. *Hydrol. Earth Syst. Sci.* 26, 4837–4851. <https://doi.org/10.5194/hess-26-4837-2022>.
- Laudon, H., Lidberg, W., Sponseller, R.A., Maher Hasselquist, E., Westphal, F., Östlund, L., Sandström, C., Järveoja, J., Peichl, M., Ågren, A.M., 2022. Emerging technology can guide ecosystem restoration for future water security. *Hydrol. Process.* 36, e14729. <https://doi.org/10.1002/hyp.14729>.
- Le Roux, G., Laverret, E., Shoty, W., 2006. Fate of calcite, apatite and feldspars in an ombrotrophic peat bog, Black Forest, Germany. *J. Geol. Soc.* 163, 641–646. <https://doi.org/10.1144/0016-764920-035>.
- Lees, K.J., Clark, J.M., Quaife, T., Khomik, M., Artz, R.R.E., 2019. Changes in carbon flux and spectral reflectance of Sphagnum mosses as a result of simulated drought. *Ecophysiology* 12, e2123. <https://doi.org/10.1002/eco.2123>.
- Lees, K.J., Artz, R.R.E., Khomik, M., Clark, J.M., Ritson, J., Hancock, M.H., Cowie, N.R., Quaife, T., 2020. Using spectral indices to estimate water content and GPP in Sphagnum moss and other peatland vegetation. *IEEE Trans. Geosci. Remote Sens.* 58, 4547–4557. <https://doi.org/10.1109/TGRS.2019.2961479>.
- Lidberg, W., Paul, S.S., Westphal, F., Richter, K.F., Lavesson, N., Melniks, R., Ivanovs, J., Ciesielski, M., Leinonen, A., Ågren, A.M., 2023. Mapping drainage ditches in forested landscapes using deep learning and aerial laser scanning. *J. Irrig. Drain. Eng.* 149, 04022051. <https://doi.org/10.1061/JIDEDH.IRENG-9796>.
- Lindén, M., Möller, P., Björck, S., Sandgren, P., 2006. Holocene shore displacement and deglaciation chronology in Norrbotten, Sweden. *Boreas* 35, 1–22. <https://doi.org/10.1080/03009480500359160>.
- Loiko, S., Klimova, N., Kuzmina, D., Pokrovsky, O., 2020. Lake drainage in permafrost regions produces variable plant communities of high biomass and productivity. *Plants* 9, 867. <https://doi.org/10.3390/plants9070867>.
- Loisel, J., Yu, Z., Beilman, D.W., Camill, P., Alm, J., Amesbury, M.J., Anderson, D., Andersson, S., Bochicchio, C., Barber, K., Belyea, L.R., Bunbury, J., Chambers, F.M., Charman, D.J., De Vleeschouwer, F., Fialkiewicz-Koziele, B., Finkelstein, S.A., Gaika, M., Garneau, M., Hammarlund, D., Hinchcliffe, W., Holmquist, J., Hughes, P., Jones, M.C., Klein, E.S., Kokfelt, U., Korhola, A., Kuhry, P., Lamarre, A., Lamentowicz, M., Large, D., Lavoie, M., MacDonald, G., Magnan, G., Mäkilä, M., Mallon, G., Mathijssen, P., Mauquoy, D., McCarrall, J., Moore, T.R., Nichols, J., O'Reilly, B., Oksanen, P., Packalen, M., Peteet, D., Richard, P.J., Robinson, S., Ronkainen, T., Rundgren, M., Sannel, A.B.K., Tarnocai, C., Thom, T., Tuittila, E.-S., Turetsky, M., Väliranta, M., van der Linden, M., van Geel, B., van Bellen, S., Vitt, D., Zhao, Y., Zhou, W., 2014. A database and synthesis of northern peatland soil properties and Holocene carbon and nitrogen accumulation. *The Holocene* 24, 1028–1042. <https://doi.org/10.1177/0959683614538073>.
- Maher, K., 2010. The dependence of chemical weathering rates on fluid residence time. *Earth Planet. Sci. Lett.* 294, 101–110. <https://doi.org/10.1016/j.epsl.2010.03.010>.
- Maher, K., von Blanckenburg, F., 2023. *The Circular Nutrient Economy of Terrestrial Ecosystems and the Consequences for Rock Weathering*. *Front. Environ. Sci.* p. 10.
- Mäkilä, M., Nieminen, T.M., Säävuori, H., Loukola-Ruskeeniemi, K., Ukonmaanaho, L., 2015. Does underlying bedrock affect the geochemistry of drained peatlands? *Geoderma* 239–240, 280–292. <https://doi.org/10.1016/j.geoderma.2014.11.002>.
- Martini, I.P., Gloschenko, W.A., 1985. Cold climate peat formation in Canada, and its relevance to Lower Permian coal measures of Australia. *Earth-Sci. Rev.* 22, 107–140. [https://doi.org/10.1016/0012-8252\(85\)90003-0](https://doi.org/10.1016/0012-8252(85)90003-0).
- McCarter, C.P.R., Wilkinson, S.L., Moore, P.A., Waddington, J.M., 2021. Ecophysiological trade-offs from multiple peatland disturbances: the interactive effects of drainage, harvesting, restoration and wildfire in a southern Ontario bog. *J. Hydrol.* 601, 126793. <https://doi.org/10.1016/j.jhydrol.2021.126793>.
- McPartland, M.Y., Kane, E.S., Falkowski, M.J., Kolka, R., Turetsky, M.R., Palik, B., Montgomery, R.A., 2019. The response of boreal peatland community composition and NDVI to hydrologic change, warming, and elevated carbon dioxide. *Glob. Chang. Biol.* 25, 93–107. <https://doi.org/10.1111/gcb.14465>.
- Mehmood, A., Akhtar, M.S., Imran, M., Rukh, S., 2018. Soil apatite loss rate across different parent materials. *Geoderma* 310, 218–229. <https://doi.org/10.1016/j.geoderma.2017.09.036>.
- Moor, H., Rydin, H., Hylander, K., Nilsson, M.B., Lindborg, R., Norberg, J., 2017. Towards a trait-based ecology of wetland vegetation. *J. Ecol.* 105, 1623–1635. <https://doi.org/10.1111/1365-2745.12734>.
- Murphy, P.N.C., Ogilvie, J., Meng, F.-R., White, B., Bhatti, J.S., Arp, P.A., 2011. Modelling and mapping topographic variations in forest soils at high resolution: a case study. *Ecol. Model.* 222, 2314–2332. <https://doi.org/10.1016/j.ecolmodel.2011.01.003>.
- Mzobe, P., Berggren, M., Pilesjö, P., Lundin, E., Olefeldt, D., Roulet, N.T., Persson, A., 2018. Dissolved organic carbon in streams within a subarctic catchment analysed using a GIS/remote sensing approach. *PLoS One* 13, e0199608. <https://doi.org/10.1371/journal.pone.0199608>.
- Nieminen, M., Hasselquist, E.M., Mosquera, V., Ukonmaanaho, L., Sallantausta, T., Sarkkola, S., 2022. Post-drainage stand growth and peat mineralization impair water quality from forested peatlands. *J. Environ. Qual.* 51, 1211–1221. <https://doi.org/10.1002/jeq2.20412>.
- Nordman, M., Peltola, A., Bilker-Koivula, M., Lahtinen, S., 2020. Past and future sea level changes and land uplift in the Baltic Sea seen by geodetic observations. *International Association of Geodesy Symposia*. Springer Berlin Heidelberg, Berlin, Heidelberg. https://doi.org/10.1007/1345_2020_124.
- Nwaishi, F., Morison, M., Plach, J., Macrae, M., Petrone, R., 2022. Carbon and nutrient stoichiometric relationships in the soil–plant systems of disturbed boreal forest peatlands within Athabasca Oil Sands Region, Canada. *Forests* 13, 865. <https://doi.org/10.3390/f13060865>.
- Økland, R.H., Økland, T., Rydgren, K., 2001. A Scandinavian perspective on ecological gradients in north-west European mires: reply to wheeler and proctor. *J. Ecol.* 89, 481–486.
- Park, T., Ganguly, S., Tømmervik, H., Euskirchen, E.S., Hogda, K.-A., Karlsen, S.R., Brovkin, V., Nemani, R.R., Myneni, R.B., 2016. Changes in growing season duration and productivity of northern vegetation inferred from long-term remote sensing data. *Environ. Res. Lett.* 11, 084001. <https://doi.org/10.1088/1748-9326/11/8/084001>.
- Peichl, M., Gažovič, M., Vermeij, I., de Goede, E., Sonnentag, O., Limpens, J., Nilsson, M.B., 2018. Peatland vegetation composition and phenology drive the seasonal trajectory of maximum gross primary production. *Sci. Rep.* 8, 8012. <https://doi.org/10.1038/s41598-018-26147-4>.
- Pettorelli, N., 2013. *The Normalized Difference Vegetation Index*. Oxford University Press.
- Piilo, S.R., Väliranta, M.M., Amesbury, M.J., Aquino-López, M.A., Charman, D.J., Gallego-Sala, A., Garneau, M., Koroleva, N., Kärrpää, M., Laine, A.M., Sannel, A.B.K., Tuittila, E.-S., Zhang, H., 2023. Consistent centennial-scale change in European sub-Arctic peatland vegetation toward Sphagnum dominance—implications for carbon sink capacity. *Glob. Chang. Biol.* 29, 1530–1544. <https://doi.org/10.1111/gcb.16554>.
- Prescott, C.E., Maynard, D.G., Laiho, R., 2000. Humus in northern forests: friend or foe? *For. Ecol. Manag.* 133, 23–36. [https://doi.org/10.1016/S0378-1127\(99\)00295-9](https://doi.org/10.1016/S0378-1127(99)00295-9).
- Räsänen, A., Aurela, M., Juutinen, S., Kumpula, T., Lohila, A., Penttilä, T., Virtanen, T., 2020. Detecting northern peatland vegetation patterns at ultra-high spatial resolution. *Remote Sens. Ecol. Conserv.* 6, 457–471. <https://doi.org/10.1002/rse2.140>.
- Rehell, S., Laitinen, J., Oksanen, J., Siira, O.-P., 2019. Mire margin to expanse gradient in part relates to nutrients gradient: evidence from successional mire basins, north Finland. *Mires Peat* 1–12. <https://doi.org/10.19189/Map.2018.OMB.353>.
- Renberg, I., Segerström, U., 1981. The initial points on a shoreline displacement curve for southern Västerbotten, dated by varve-counts of lake sediments. *Striae* 14, 174–176.
- Richardson, C.J., 1985. Mechanisms controlling phosphorus retention capacity in freshwater wetlands. *Science* 228, 1424–1427. <https://doi.org/10.1126/science.228.4706.1424>.
- Rinne, J., Tuovinen, J.-P., Klemetsson, L., Aurela, M., Holst, J., Lohila, A., Weslien, P., Vestin, P., Lakomiec, P., Peichl, M., Tuittila, E.-S., Heiskanen, L., Laurila, T., Li, X., Alekseychik, P., Mammarella, I., Ström, L., Crill, P., Nilsson, M.B., 2020. Effect of the 2018 European drought on methane and carbon dioxide exchange of northern mire ecosystems. *Philos. Trans. R. Soc. B Biol. Sci.* 375, 20190517. <https://doi.org/10.1098/rstb.2019.0517>.
- Romanov, V.V., 1968. *Hydrographics of bogs*. Israel Programme for Scientific Translation, Jerusalem.
- Rouse Jr., J.W., Haas, R.H., Schell, J.A., Deering, D.W., 1973. *Monitoring the vernal advancement and retrogradation (green and wave effect) of natural vegetation*. No. NASA-CR-132982.
- Ruppel, M., Väliranta, M., Virtanen, T., Korhola, A., 2013. Postglacial spatiotemporal peatland initiation and lateral expansion dynamics in North America and northern Europe. *The Holocene* 23, 1596–1606. <https://doi.org/10.1177/0959683613499053>.
- Rydin, H., Sjörs, H., Löfroth, M., 1999. 7. Mires. *Acta Phytogeogr. Suec.* 84, 91–112.
- Rydin, H., Jørgensen, J., Bennett, K., 2013. *The Biology of Peatlands*. 2e. Oxford University Press.
- Sjörs, H., Gunnarsson, U., 2002. Calcium and pH in north and central Swedish mire waters. *J. Ecol.* 90, 650–657. <https://doi.org/10.1046/j.1365-2745.2002.00701.x>.
- Soomers, H., Karssenberg, D., Verhoeven, J.T.A., Verweij, P.A., Wassen, M.J., 2013. The effect of habitat fragmentation and abiotic factors on fen plant occurrence. *Biodivers. Conserv.* 22, 405–424. <https://doi.org/10.1007/s10531-012-0420-1>.
- Sponseller, R.A., Blackburn, M., Nilsson, M.B., Laudon, H., 2018. Headwater mires constitute a major source of nitrogen (N) to surface waters in the boreal landscape. *Ecosystems* 21, 31–44. <https://doi.org/10.1007/s10021-017-0133-0>.
- Starr, M., Lindroos, A.-J., 2006. Changes in the rate of release of Ca and Mg and normative mineralogy due to weathering along a 5300-year chronosequence of boreal forest soils. *Geoderma* 133, 269–280. <https://doi.org/10.1016/j.geoderma.2005.07.013>.
- Stroeven, A.P., Hättetrand, C., Klemm, J., Heyman, J., Fabel, D., Fredin, O., Goodfellow, B.W., Harbor, J.M., Jansen, J.D., Olsen, L., Caffee, M.W., Fink, D., Lundqvist, J., Rosqvist, G.C., Strömberg, B., Jansson, K.N., 2016. Deglaciation of Fennoscandia. *Quat. Sci. Rev.* 147, 91–121. <https://doi.org/10.1016/j.quascirev.2015.09.016> Special Issue: PAST Gateways (Palaeo-Arctic Spatial and Temporal Gateways).
- Svensson, J.S., Jørgensen, J.K., 2001. Structure and dynamics of an undisturbed old-growth Norway spruce forest on the rising Bothnian coastline. *For. Ecol. Manag.* 151, 67–79. [https://doi.org/10.1016/S0378-1127\(00\)00697-6](https://doi.org/10.1016/S0378-1127(00)00697-6).

- Tahvanainen, T., 2011. Abrupt ombrotrophication of a boreal aapa mire triggered by hydrological disturbance in the catchment. *J. Ecol.* 99, 404–415. <https://doi.org/10.1111/j.1365-2745.2010.01778.x>.
- The Swedish Meteorological and Hydrological Institute, 2022. <https://www.smhi.se/data/meteorologi/ladda-ner-meteorologiska-observationer#param=airtemperatureInstant,stations=core>.
- Tiselius, A.K., Lundbäck, S., Lönnell, N., Jansson, R., Dynesius, M., 2019. Bryophyte community assembly on young land uplift islands – dispersal and habitat filtering assessed using species traits. *J. Biogeogr.* 46, 2188–2202. <https://doi.org/10.1111/jbi.13652>.
- Tuittila, E.-S., Juutinen, S., Frolking, S., Väliaranta, M., Laine, A.M., Miettinen, A., Seväkivi, M.-L., Quillet, A., Merilä, P., 2013. Wetland chronosequence as a model of peatland development: vegetation succession, peat and carbon accumulation. *The Holocene* 23, 25–35.
- Tuyishime, J.R.M., Adediran, G.A., Olsson, B.A., Spohn, M., Hillier, S., Klysubun, W., Gustafsson, J.P., 2022. Phosphorus abundance and speciation in acid forest Podzols – effect of postglacial weathering. *Geoderma* 406, 115500. <https://doi.org/10.1016/j.geoderma.2021.115500>.
- Vincent, A.G., Schleucher, J., Gröbner, G., Vestergren, J., Persson, P., Jansson, M., Giesler, R., 2012. Changes in organic phosphorus composition in boreal forest humus soils: the role of iron and aluminium. *Biogeochemistry* 108, 485–499. <https://doi.org/10.1007/s10533-011-9612-0>.
- Walker, L.R., Wardle, D.A., Bardgett, R.D., Clarkson, B.D., 2010. The use of chronosequences in studies of ecological succession and soil development: Chronosequences, succession and soil development. *J. Ecol.* 98, 725–736. <https://doi.org/10.1111/j.1365-2745.2010.01664.x>.
- Wallander, H., Thelin, G., 2008. The stimulating effect of apatite on ectomycorrhizal growth diminishes after PK fertilization. *Soil Biol. Biochem.* 40, 2517–2522. <https://doi.org/10.1016/j.soilbio.2008.06.011>.
- Wood, T., Bormann, F.H., Voigt, G.K., 1984. Phosphorus cycling in a northern hardwood forest: biological and chemical control. *Science* 223, 391–393. <https://doi.org/10.1126/science.223.4634.391>.
- Worrall, F., Boothroyd, I., Clay, G.D., Moody, C.S., Heckman, K., Burt, T.P., Rose, R., 2022. Constraining the carbon budget of peat ecosystems: application of stoichiometry and enthalpy balances. *J. Geophys. Res. Biogeosci.* 127, e2022JG007003. <https://doi.org/10.1029/2022JG007003>.
- Yuan, W., Liu, S., Dong, W., Liang, S., Zhao, S., Chen, J., Xu, W., Li, X., Barr, A., Andrew Black, T., Yan, W., Goulden, M.L., Kulmala, L., Lindroth, A., Margolis, H.A., Matsuura, Y., Moors, E., van der Molen, M., Ohta, T., Pilegaard, K., Varlagin, A., Vesala, T., 2014. Differentiating moss from higher plants is critical in studying the carbon cycle of the boreal biome. *Nat. Commun.* 5, 4270. <https://doi.org/10.1038/ncomms5270>.
- Zevenbergen, L.W., Thorne, C.R., 1987. Quantitative analysis of land surface topography. *Earth Surf. Process. Landf.* 12, 47–56. <https://doi.org/10.1002/esp.3290120107>.
- Zhao, Z., Ashraf, M.I., Keys, K.S., Meng, F.-R., 2013. Prediction of soil nutrient regime based on a model of DEM-generated clay content for the province of Nova Scotia, Canada. *Can. J. Soil Sci.* 93, 193–203. <https://doi.org/10.4141/cjss2012-016>.